Redox Biology 51 (2022) 102277

Contents lists available at ScienceDirect

Redox Biology

journal homepage: www.elsevier.com/locate/redox

Mitochondrial depletion of glutaredoxin 2 induces metabolic dysfunction-associated fatty liver disease in mice

Valeria Scalcon [a,1], Alessandra Folda [a], Maria Giovanna Lupo [b], Federica Tonolo [a], Naixuan Pei [c], Ilaria Battisti [a,d], Nicola Ferri [b], Giorgio Arrigoni [a,d], Alberto Bindoli [e], Arne Holmgren [c,2], Lucia Coppo [c,**,1], Maria Pia Rigobello [a,*]

[a] Department of Biomedical Sciences, University of Padova, 35131, Padova, Italy
[b] Department of Medicine, University of Padova, 35121, Padova, Italy
[c] Department of Medical Biochemistry and Biophysics, Karolinska Institutet, SE-17165, Stockholm, Sweden
[d] Proteomics Center, University of Padova and Azienda Ospedaliera di Padova, 35129, Padova, Italy
[e] Institute of Neuroscience, CNR c/o Department of Biomedical Sciences, University of Padova, 35131, Padova, Italy

ARTICLE INFO

Keywords:
Glutaredoxin 2
Mitochondria
Lipid metabolism
ROS production
MAFLD
Mouse model

ABSTRACT

Glutaredoxin 2 (Grx2) is a glutathione-dependent oxidoreductase that facilitates glutathionylation/deglutathionylation of target proteins. The main variants of Grx2 are the mitochondrial Grx2a and the cytosolic Grx2c. The aim of this study was to investigate the specific role of mitochondrial Grx2 *in vivo* using a mitochondrial Grx2 depleted (mGD) mouse model. mGD mice displayed an altered mitochondrial morphology and functioning. Furthermore, the lack of Grx2 in the mitochondrial compartment is responsible for increased blood lipid levels under a normal diet, a metabolic dysfunction-associated fatty liver disease (MAFLD) phenotype and a decreased glycogen storage capacity. In addition, depleting Grx2a leads to an alteration in abundance and in glutathionylation pattern of different mitochondrial enzymes, highlighting the selective role of Grx2 in the regulation of metabolic pathways. Overall, our findings identify the involvement of mitochondrial Grx2a in the regulation of cell metabolism and highlight a previously unknown association between Grx2 and MAFLD.

1. Introduction

Thiol redox regulation is crucial for the physiology of mitochondria and is involved in the modulation of various functions of these organelles such as permeability transition and activity of the electron transport chain [1–3].

Glutathionylation is a tightly controlled and highly specific post-translational modification (PTM) involving reversible binding of glutathione (GSH) to a reactive protein cysteine [4,5]. Noteworthy, cysteine residues of mitochondrial proteins are particularly susceptible to glutathionylation due to the unique physical properties of the matrix: the concentration of reduced glutathione around 5 mM and the slightly alkaline environment which promote the formation of the thiolate form of cysteines [6]. In mitochondria, this reaction is mediated by glutaredoxin 2 (Grx2), a thiol oxidoreductase discovered in 2001 [7,8]. Two major Grx2 isoforms are known, encoded by the same gene (*GLRX2*): Grx2a (mitochondrial) and Grx2c (cytosolic) [9,10]. Grx2 contains the active site sequence CSYC, which makes Grx2 catalytic site more flexible compared to other glutaredoxins [11]. Due to this feature, Grx2 is also a substrate of thioredoxin reductase [12] and can coordinate a [2Fe–2S] iron-sulfur center forming a dimer [13]. Of note, the iron-sulfur cluster represents a redox sensor and, consequently, Grx2 enzymatic activity is tightly regulated in response to fluctuations in the redox buffering capacity of the mitochondrial matrix [14,15]. In particular, oxidative stress conditions were shown to destabilize the holo-dimer leading to the release of active Grx2 monomers [14,15]. The significance of the iron-sulfur binding and of the glutathionylation process still needs to be defined. So far little is known about the role of Grx2a-mediated glutathionylation in mitochondria and the impact of these modifications on cellular metabolism. To clarify this process, we employed a mouse

* Corresponding author.
** Corresponding author.
E-mail addresses: lucia.coppo@ki.se (L. Coppo), mariapia.rigobello@unipd.it (M.P. Rigobello).
[1] These authors contributed equally.
[2] Deceased January 6th 2020.

https://doi.org/10.1016/j.redox.2022.102277
Received 12 January 2022; Received in revised form 18 February 2022; Accepted 26 February 2022
Available online 2 March 2022

model selectively lacking Grx2 in the mitochondrial compartment (mitochondrial Grx2 depleted, shortened as mGD). The deletion of the signal peptide gene segment caused a lack of Grx2 expression in the mitochondria but did not affect the expression of the protein in the cytosol allowing us to study the role of Grx2 in the mitochondrial compartment.

Metabolic dysfunction-associated fatty liver disease (MAFLD) is a liver pathology characterized by an increase in lipid deposition in the hepatocytes known as hepatic steatosis [16]. The prevalence of MAFLD is increasing rapidly with the growing epidemics of diabetes and obesity, and is thought to affect a large part of the world population [17,18]. Unfortunately, the complexity of MAFLD impinges on the establishment of appropriate protocols for its management and on the development of effective therapies. Thus, the study of the specific mechanisms involved in its pathogenesis is fundamental for the dissection of the disease and consequently for its correct treatment.

Here, we investigated the early changes in metabolic pathways associated with the depletion of Grx2a. mGD mice fed with standard chow diet showed a spontaneous increase in body weight and an accumulation of lipid droplets in the liver compared to wild type (WT) mice. This phenotype was associated with an increase in blood lipid levels and impairment of liver mitochondria functions. Importantly, we report here a mass spectrometry analysis showing the effect of Grx2 absence on the expression and glutathionylation of specific pathways and mitochondrial enzymatic systems. In addition, our data show that Grx2a deficiency largely affects the overall lipid metabolism. This evidence indicates the involvement of Grx2a in the crosstalk between mitochondrial redox regulation and lipid metabolism, in particular for the hepatic physiology, suggesting a mechanistic importance of Grx2a in the development of MAFLD.

2. Materials and methods

2.1. Generation of the mouse model and animal housing

The mouse model with a deletion of the mitochondrial localization signal of glutaredoxin 2 (mGD, mitochondrial-Grx2-Depleted) was made at the Central Institute for Experimental Animals (CIEA; http://www.ciea.or.jp), Japan. This mouse model was generated by targeting exons 1c, 1a and 2 of *Glrx2* gene and replacing them by a Neomycin cassette which was subsequently excised in C57BL/6J background (See Fig. S1). Mice received commercial rodent food (standard chow diet) and neutral pH water *ad libitum* and were maintained under a 12 h light/12 h dark cycle under constant room temperature (22 ± 1 °C) and humidity conditions (40–60%). The experiments were carried out using males at the indicated age. For fasting experiments, a 12 h food deprivation was carried out overnight. Animal housing, handling and experimentation were approved by the Regional Animal Ethics Committee of Northern Stockholm and by the Ethical Committee for Animal Care and Use of the University of Padova (OPBA).

2.2. RNA isolation with TRIzol® reagent

The tissue was homogenized directly in TRIzol® reagent with a glass homogenizer following the data sheet protocol (Thermo Fisher Scientific, Waltham, MA, USA). RNA was dissolved in RNase-free water and stored at −80 °C and later reverse transcribed using Maxima First Strand cDNA synthesis kit (Thermo Fisher Scientific). Genotyping was performed using DreamTaq Green PCR Master Mix kit (Thermo Fisher Scientific) and the primers used are listed below (Table 1). The genes involved in the cholesterol metabolism, lipid metabolic pathways and inflammation markers were analyzed by RT-qPCR using luminaris Color HiGreen qPCR Master Mix (Thermo Fisher Scientific). The primers used are listed below (Table 2).

Table 1
Primers used for genotyping.

Primers	Reverse 5′-3′	Forward 5′-3′
Neomycin	GCC CAG TCA TAG CCG AAT AG	CGT TGG CTA CCC GTG ATA TT
Glrx2-exon1		ATG GGA AAC AGC ACA TCG TCG
Glrx2-exon4	CAG AGG CAG CAA TTT CCC	
Glrx2-exon2		TGG GAA ACA GCA CAT CGT C
Glrx2-exon3		CTA ACA ATT GTG TGG TGA TCT TC
β-Actin	CCT CAC CAA CTG TAC CAT CAG	GGC TGT ATT CCC CTC CAT CG

Table 2
Primers used for cholesterol and fatty acids metabolic genes and inflammation markers.

Primers	Reverse 5′-3′	Forward 5′-3′
Cyp7a1	GGT ATG GAA TCA ACC CGT TGT C	GGG ATT GCT GTG GTA GTG AGC
Ldlr	CCA TCT AGG CAA TCT CGG TCT C	TCA GAC GAA CAA GGC TGT CC
Hmgcr	CCG CGT TAT CGT CAG GAT GA	TGT TCA CCG GCA ACA ACA AGA
Srebf2	CAC CAG GGT TGG CAC TTG AA	GTT GAC CAC GCT GAA GAC AGA
Cpt1a	CAC CAG TGA TGA TGC CAT TCT	CTC CGC CTG AGC CAT GAA G
Cd36	GTT GGT TGC CAA GGG AAT TG	TGA TGG GTC TTC ACC AGA AAT AG
Scd1	CGG GAT TGA ATG TTC TTG TCG T	TTC TTG CGA TAC ACT CTG GTG C
Fasn	GCT TGG TCC TTT GAA GTC GAA GA	AGA GAT CCC GAG ACG CTT CT
Acc1	GGG ATG GCA GTA AGG TCA AA	ACA TTC CGA GCA AGG GAT AAG
Srebf1	CAT AGG GGG CGT CAA ACA G	GAT GTG CGA ACT GGA CAC AG
Vdr	GGG CTA CTA CAG AGG AAG AAA TG	TCC TCC TGA CTC TTC ACT CTA C
Glrx1	AGA AGA CCT TGT TTG AAA GGC A	GCT CAG GAG TTT GTG AAC TGC
Pdha1	TGA TCC GCC TTT AGC TCC ATC	GAA ATG TGA CCT TCA TCG GCT
Acc2 (Acacb)	GCT TGG CAG GGA GTT CCT C	CGC TCA CCA ACA GTA AGG TGG
Crat	CCT TGA GGT AAT AGT CCA GGG A	GCT GCC AGA ACC GTG GTA AA
Pparg	AGG CTC CAT AAA GTC ACC AAA G	CTG GCC TCC CTG ATG AAT AAA G
Apoa1	TCT CCT GTC TCA CCC AAT CT	CTC TGG GTT CAA CCG TTA GTC
HK4	GCA ACA TCT TTA CAC TGG CCT	TGA GCC GGA TGC AGA AGG A
IL-1β	GCT TGG GAT CCA CAC TCT CC	GCT GAA AGC TCT CCA CCT CA
IL-6	GAC AGG TCT GTT GGG AGT GG	CTC TGC AAG AGA CTT CCA TCC A
TNF-α	CTG ATG AGG GAG GCC ATT	GCC TCT TCT CAT TCC TTG
NFKB1	ATC ACT TCA ATG GCC TCT GTG TAG	GAA ATT CCC TGA TCC AGA CAA AAA C
Lep	TGG GAG ACA GGG TTC TAC TT	GGT TGA TCT CAC AAT GCG TTT C
Vdr	GGG CTA CTA CAG AGG AAG AAA TG	TCC TCC TGA CTC TTC ACT CTA C
β-Actin	CCA GTT GGT AAC AAT GCC ATG T	GGC TGT ATT CCC CTC CAT CG

2.3. Immunogold labeling of Grx2 in liver sections

For immunostaining of liver sections, the post-embedding immunogold method was applied. The samples were fixed in 4%

paraformaldehyde in phosphate-buffered saline (PBS) 1X solution, dehydrated and embedded in LR White Resin (Craig and Miller 1984) and polymerized at 58 °C. Ultrathin sections (90–100 nm) were placed on 200 mesh formvar-coated nickel grids, treated with blocking solution (0.5% bovine serum albumin (BSA), 0.1% Saponin, PBS 1X), then incubated with rabbit polyclonal *anti*-GLRX2 antibody diluted 1:50 (see Ab list) overnight at 4 °C. Ab binding was detected using a goat anti-rabbit secondary Ab (Sigma-Aldrich G7402) coupled to gold particles 10 nm diameter diluted 1:100. After staining with uranyl acetate and lead citrate, liver sections were analyzed at a FEI Tecnai G12 transmission electron microscope (TEM) operating at 100 KV. The images were captured with a Veleta (Olympus Soft Imaging System) digital camera. Controls were performed by omitting primary Ab, which resulted in the absence of cross-reactivity.

2.4. Mitochondria isolation

Mouse liver, heart and kidney mitochondria were isolated by differential centrifugation following the method of Myers and Slater [19]. Mice were sacrificed by cervical dislocation and the different organs were explanted and dipped in ice-cold isolation buffer (220 mM sucrose, 70 mM mannitol, 0.1 mM EDTA, 5 mM Hepes-Tris (pH 7.0)). Once removed blood traces, the organs were minced and homogenized. For the heart, the connective tissue was partially removed by fiberglass filtering. Afterwards, the homogenates were centrifuged at 700×*g* for 10 min at 4 °C and the obtained supernatants were centrifuged at 10000×*g* for 15 min at 4 °C. The pellets (mitochondrial fractions) were suspended and centrifuged at 10000×*g* for 15 min at 4 °C in the isolation buffer without EDTA.

For isolation of brain mitochondria, the procedure utilized followed standard protocols [20]. After cervical dislocation, the complete brain was immediately removed and placed in an ice-cold extraction buffer (125 mM sucrose, 250 mM mannitol, 10 mM EGTA, 0.01% BSA, 1x protease inhibitors (Complete, Roche, Mannheim, DE), 10 mM Hepes-Tris (pH 7.2)) and rinsed twice. Then, the brain was minced and gently homogenized using a dounce. The homogenate was centrifuged at 700×*g* for 10 min at 4 °C, the supernatant was centrifuged at 700×*g* for 10 min at 4 °C and then at 10000×*g* for 15 min at 4 °C. The pellet was suspended in ice-cold extraction buffer with 0.02% digitonin (final concentration). The centrifugation at 10000×*g* for 15 min at 4 °C was repeated and the final pellet was dissolved in a small volume of extraction buffer and subjected to protein determination. Concentrations of mitochondrial proteins were estimated with the Bradford method [21].

2.5. ORO staining for lipid detection

Once sacrificed, the liver was promptly withdrawn from the mouse. A slice of liver was cut and frozen in OCT (Tissue-Tek, Sakura Finetek, USA) using liquid nitrogen. Then, frozen sections were cut at 8–10 μm in a cryostat at −20 °C. Afterwards, air dried sections were washed with distilled water and stained with freshly prepared Oil Red O working solution as reported previously [22]. Slices were rinsed with distilled water and nuclei were stained with hematoxylin. After several washes with distilled water, sections in aqueous mountant were observed using a DMR Fluorescence Microscope (Leica, Wetzlar, Germany).

2.6. TEM imaging of isolated liver mitochondria and liver or heart sections

WT and mGD liver mitochondria, liver and heart biopsies were immersed into the fixative solution formed by 2.5% glutaraldehyde, 2% paraformaldehyde in 0.1 M sodium cacodylate buffer (pH 7.4) and finely cut. The specimens were placed at 4 °C overnight and then washed with cacodylate buffer 3 times for 10 min at 4 °C. Afterwards, 1% osmium tetroxide in 0.1 M sodium cacodylate buffer (pH 7.4) was added for 1 h at 4 °C. Samples were washed twice for 10 min with the buffer at 4 °C and with distilled water for 10 min at 4 °C, then dehydrated in a graded ethanol series and infiltrated with transitional solvent composed by propylene oxide followed by epoxy resin infiltration. Samples were embedded in pure epoxy resin which was allowed to polymerize at 60 °C for 2 days. Ultrathin sections (60–70 nm) were obtained with an Ultrotome V (LKB) ultramicrotome, counterstained with uranyl acetate and lead citrate and finally, slices were observed using a Transmission Electron Microscope FEI Tecnai G12.

2.7. Determination of ROS production

WT and mGD mouse liver mitochondria (0.5 mg/mL) were incubated at 25 °C in a 96-well plate with 20 mM Hepes-Tris buffer (pH 7.4) containing 100 mM sucrose, 50 mM KCl, 0.5 mM NaKPi and 5 mM succinate with or without 1 μM cyclosporin A (CsA). Formation of H_2O_2 was detected fluorimetrically with 20 μM Amplex™ Red (Invitrogen, Carlsbad, CA, USA) in the presence of 11 nM horseradish peroxidase (HRP) using a Tecan Infinite M200 PRO plate reader (Tecan, Männedorf, CH) (λ_{Ex} = 530 nm, λ_{Em} = 590 nm).

2.8. Measurement of the mitochondrial membrane potential

The mitochondrial membrane potential of mouse liver mitochondria was estimated by means of the fluorescent dye rhodamine 123 (Sigma-Aldrich, St. Louis, MO, USA). Mitochondrial proteins (0.5 mg/mL) were incubated at 25 °C in 20 mM Hepes-Tris buffer (pH 7.4), 100 mM sucrose, 50 mM KCl, 1 mM $MgCl_2$, and 1 mM NaH_2PO_4 containing 12.5 μM rotenone. Mitochondria were treated with 5 mM succinate or 5 μM palmitoylcarnitine as oxidizable substrate in the presence or absence of EGTA or CsA, as indicated. Fluorescence was estimated (λ_{Ex} = 485 nm, λ_{Em} = 527 nm) using a Tecan Infinite M200 PRO plate reader. In this method, the membrane potential increase is directly related to the decrease of the probe fluorescence. The ratio between the fluorescence recorded before and after the addition of the substrate was calculated and compared between WT and mGD mice.

2.9. Estimation of mitochondrial swelling

Mitochondrial swelling was followed spectrophotometrically as decrease of the optical density at 540 nm. Briefly, liver mitochondria (0.25 mg/mL) were incubated at 25 °C in 5 mM Hepes-Tris buffer (pH 7.4), 213 mM mannitol, 71 mM sucrose, containing 5 mM succinate, 5 μM rotenone and 2.5 μM oligomycin in the presence or absence of calcium chloride and/or EGTA. The absorbance at 540 nm was monitored spectrophotometrically.

2.10. Determination of the oxygen consumption

Oxygen consumption of mouse liver mitochondria was measured polarographically, utilizing a Clark-type oxygen electrode inserted in a water-jacketed chamber (27 °C) with constant stirring. Mouse liver mitochondria (1 mg/mL) were incubated at 27 °C in 20 mM Hepes-Tris buffer (pH 7.4), 100 mM sucrose, 50 mM KCl, 1 mM $MgCl_2$, 1 mM NaH_2PO_4 and 20 μM EGTA. Respiration was started by the addition of either 7.5 mM succinate or the combination 7.5 mM glutamate +3.75 mM malate or 20 μM palmitoylcarnitine (state 4). Then, 0.2 mM ADP was added (state 3). Finally, 0.25 μM trifluoromethoxy carbonylcyanide phenylhydrazone (FCCP) was added to measure the maximal respiration rate (state 3u). The oxygen consumption was calculated in nmoles of $O_2 \cdot sec^{-1}$ mg^{-1} protein.

2.11. Assessment of total thiols

Liver, heart, brain and kidney mitochondria (0.25 mg of proteins) were dissolved with 0.2 M Tris-HCl buffer (pH 8.1), 1% SDS and 10 mM

EDTA to a final volume of 1 mL. Then, 3 mM DTNB was added to titrate thiol groups and the absorbance increase was monitored at 412 nm for 5 min [23]. The amount of thiols was determined by subtracting the background optical density observed before the addition of DTNB.

2.12. Total glutathione and GSSG estimation

Aliquots of mitochondria (0.5 mg) isolated from fasted 3 months-old mGD and WT mice, were deproteinized with 2 mL of 6% *meta*-phosphoric acid. After 20 min at 4 °C, samples were centrifuged at 15800×*g* for 10 min at 4 °C. Supernatants were neutralized with 15% Na_3PO_4 and utilized for total glutathione estimation [24]. For measurement of oxidized glutathione, sample aliquots were treated with 2% 2-vinylpyridine for 40 min before performing the assay in order to derivatize reduced glutathione and quantify only oxidized glutathione.

2.13. Quantification of the protein-bound iron pool in WT and mGD mouse liver mitochondria

Liver mitochondria were obtained following the protocol described above. Soon after isolation, 0.5 mg of mouse liver mitochondria (MLM) were treated with 600 μL of 6% *meta*-phosphoric acid for 30 min at 4 °C in order to obtain the acid-labile and the protein-bound iron pools. After incubation, samples were centrifuged at 15800×*g* for 10 min at 4 °C, the pellet was mineralized and the total amount of iron was estimated by atomic absorption spectroscopy. Briefly, samples were subjected to five cycles of freezing-thawing at −20/+32 °C of 20 min, mineralized in 200 μL of highly purified nitric acid (Fe: ≤0.01 mg/kg) plus 200 μL H_2O_2 and then transferred into a microwave Teflon vessel before being subjected to the standard procedure using a speed wave MWS-3 Berghof instrument (Berghof, Eningen, Germany). Fe content of each sample was determined using a Varian AA Duo graphite furnace atomic absorption spectrometer (Varian, Palo Alto, CA, USA) at the wavelength of 248.3 nm.

2.14. Measurement of lipid peroxidation of liver mitochondria via malondialdehyde (MDA) quantification

Equal amounts of WT and mGD MLM were treated with 1 mL of 0.1 N H_2SO_4 and 150 μL of 10% phosphotungstic acid (PTA) for 10 min at room temperature. Then, samples were centrifuged at 15800×*g* for 10 min at 4 °C. The supernatants were discarded and the pellets were resuspended with 1 mL of 0.1 N H_2SO_4 and 150 μL of PTA and again centrifuged as described above. Afterwards, the pellets were dissolved with 350 μL of a medium composed by 0.25% NONIDET P-40, 0.01% BHT, 0.17% thiobarbituric acid and incubated at 95 °C for 60 min. At the end, samples were ice-cooled for 5 min and centrifuged at 15800×*g* for 10 min. Supernatants were treated with 400 μL of *n*-butanol, vigorously mixed and centrifuged at 15800×*g* for 15 min. The fluorescence of the upper phase was estimated (λ_{Ex}: 530 nm; λ_{Em}: 590 nm) using a Tecan Infinite M200 PRO plate reader (Tecan, Männedorf, CH).

2.15. Western blot analysis

Isolated liver mitochondria were lysed with a modified Radioimmunoprecipitation assay (RIPA) buffer (50 mM Tris-HCl buffer (pH 7.4), 150 mM NaCl, 1 mM EDTA, 0.1% SDS, 1% Triton X100, 0.5% DOC, 1 mM NaF and 0.1 mM phenylmethylsulfonyl fluoride (PMSF)) and incubated for 40 min at 4 °C. Then, 20 μg of the lysates were subjected to 12% acrylamide/bis-acrylamide SDS-PAGE and to Western blot analysis. For the determination of protein phosphorylation state, phosphatase inhibitor tablets (PhosSTOP, Sigma-Aldrich, St. Louis, MO, USA) and 10 mM NaF were added to the media of all the processing steps in order to prevent the activity of phosphatases.

For glutathionylation experiments 20 μg of each sample was loaded on a gradient 4–12% SDS-PAGE (Any kD™ Mini-PROTEAN® TGX™ Precast Protein Gels, Biorad, Hercules, CA, USA) and probed with the *anti*-GSH antibody (Gentaur, see Table 3). Ponceau staining and TOM20 were used as loading controls.

The detection was performed using UVITEC Alliance Q9 mini chemiluminescence imaging detector (UVITEC, Cambridge, UK) and analyzed via NineAlliance software for band quantification.

In Fig. S8 the uncut Western blot membranes are reported.

2.16. PAS (Periodic Acid Schiff) staining of glycogen content

Liver slices from fed or fasted WT and mGD mice were fixed in 10% formalin and included in paraffin. Then, paraffin sections were cut at 5 μm, deparaffinized and hydrated to water. Afterwards, slices were oxidized in 0.5% periodic acid solution for 5 min, rinsed in distilled water and placed in Schiff reagent for 15 min. At the end of incubation, slices were washed in tap water for 5 min, counterstained in Mayer's hematoxylin for 5 min and washed again in tap water for 5 min. Finally, slices were dehydrated and coverslip mounted using Canada balsam. The following day, the slices were observed using a DM 5000 B microscope Leica with a 20X objective.

2.17. Quantitative proteomic analysis of glutathionylated proteins

Liver mitochondria of 3 months-old WT and mGD mice were isolated after overnight fasting as reported above, using the mitochondrial isolation buffer (220 mM sucrose, 70 mM mannitol, 0.1 mM EDTA, 5 mM Hepes-Tris, pH 7.0) in the presence of 30 mM iodoacetamide. Equal amounts of WT and mGD mitochondrial proteins (300 mg) were diluted and lysed in a 1:1 solution composed of RIPA buffer and mitochondrial isolation buffer. Next, desalting using Microspin™ G-25 Columns (General Electric, Boston, MA, USA) and pre-clearing with Protein A/G PLUS-Agarose (Santa Cruz Biotechnology, Dallas, TX, USA) were performed. Afterwards, 20 μL of *anti*-GSH primary antibody corresponding to 2 μg (Santa Cruz Biotechnology, see Table 3) were added to each sample and incubation was performed overnight at 4 °C with stirring. Then, 20 μL of Protein A/G PLUS-Agarose were added for 1 h at 4 °C and proteins precipitated at 15800×*g* for 2 min. Immunoprecipitated proteins were digested with the Filter-Aided Sample Preparation (FASP) method. Briefly, samples were mixed with Buffer A (8 M Urea, 100 mM Tris-HCl, pH 8.5) up to 200 μL, loaded into centrifugal ultrafiltration units with a nominal molecular weight cutoff of 10 kDa (Vivacon 500, Sartorius, Göttingen, Germany) and centrifuged at 18600×*g* for 15 min. After discarding the flow-through, filters were washed twice with 200 μL

Table 3
List of the primary antibodies utilized.

Antibody	Brand	Commercial code
Grx2	MyBioSource	MBS176047
Grx2	IMCO	AGRX-02
GR	Santa Cruz Biotechnology	sc-133245
Trx1	Santa Cruz Biotechnology	sc-20146
Trx2	Santa Cruz Biotechnology	sc-50336
TrxR1	Santa Cruz Biotechnology	sc-28321
TrxR2	MyBioSource	837093
SOD2	Santa Cruz Biotechnology	sc-137254
TXNIP	NovusBio	NBP154578SS
GAPDH	Santa Cruz Biotechnology	sc-32233
TOM20	Santa Cruz Biotechnology	sc-11415
GSH	Gentaur	PAA294G
GSH (IP)	Santa Cruz Biotechnology	sc-52399
Ins-R	Cell Signaling	3020S
p-Ins-R (Tyr1135/1136)	Cell Signaling	3024S
p-AKT (Ser473)	Cell signaling	9271S
AKT	Cell signaling	9272S
p-GS (Ser641)	Cell signaling	47043
GS	Cell signaling	3886
TIM23	BD Transduction laboratories	611222
HSP90	Abcam	ab13492

of buffer A by centrifuging at 18600×*g* for 15 min to keep proteins denatured and remove possible low MW compounds that might interfere with the MS analysis. Protein disulfide bridges were reduced by adding 200 μL of 50 mM dithiothreitol (Fluka, Sigma-Aldrich, St. Louis, MO, USA) in buffer A and incubating the samples at 55 °C for 30 min. After centrifugation, to alkylate free thiol groups, 100 μL of 50 mM iodoacetamide (Sigma-Aldrich) in buffer A were added, and samples were incubated for 20 min in the dark. Filter units were washed twice with 100 μL of buffer A then, to have the samples in a buffer suitable for enzymatic digestion, other two additional washing steps were performed with 100 μL of 100 mM ammonium bicarbonate and 50 mM ammonium bicarbonate (Sigma-Aldrich), respectively, by centrifuging at 18600×*g* for 10 min.

Protein digestion was carried out at 37 °C overnight with 0.24 μg of Sequencing Grade Modified Trypsin (Promega, Madison, WI, USA) (8 ng/μL in 50 mM ammonium bicarbonate). Peptides were collected by centrifugation at 18600×*g* for 10 min, followed by two washes with 100 μL of 50 mM ammonium bicarbonate. Samples were acidified with 1 μL of formic acid (FA, Sigma-Aldrich) and diluted to 1 mL with 0.1% FA, prior to desalting with C18 cartridges (Sep-Pak, C18, Waters, Milford, MA, USA) according to manufacturer's instructions. Finally, samples were dried under vacuum and stored at −20 °C. LC-MS/MS analysis was performed with a LTQ Orbitrap XL (Thermo Fisher Scientific) interfaced with a nano-HPLC Ultimate 3000 (Dionex - Thermo Fisher Scientific). Samples were suspended in 15 μL of 3% acetonitrile (ACN)/0.1% FA and for each sample 4 μL were loaded into a trap column (NanoEase Symmetry300, C18, 5 μm, Waters) at a flow rate of 8 μL/min. The peptide mixture was separated in a pico-frit capillary column (11 cm, 75 μL internal ID, 15 μm tip, New Objective, Littleton, MA, USA) packed in-house with C18 material (*ReproSil*, 300 Å, 3 μm) using a linear gradient of ACN/0.1% FA from 3 to 40% in 25 min with a flow rate of 250 nL/min. Ion source capillary was set to 200 °C and spray voltage was fixed at 1.3–1.4 kV. The instrument operated in a data-dependent mode, with a full scan in the Orbitrap (60000 resolution) in the 300–1700 *m/z* range, followed by MS/MS scans of the 10 most intense ions acquired at lower resolution in the linear trap. Each sample was acquired twice under identical instrumental conditions.

Raw MS data files were processed with MaxQuant software v.1.5.1.2, interfaced with the Andromeda search engine. Proteins search was done against the Mouse section of the UniProt database (*Mus musculus*, version 2020-09-30, 55494 entries), and trypsin was set as enzyme with up to 2 missed cleavages allowed. Carbamidomethylation of cysteines and oxidation of methionines were set as fixed and variable modifications, respectively. A minimum of two peptides was required for protein identification, and a false discovery rate (FDR) of 0.01, both at the peptide and protein level, was used to filter the results. Intensity values as calculated by the software were used to evaluate differences in protein abundances between WT and mGD samples: mGD/WT ratios were converted into log2 values and a Z-test was performed. Proteins were considered significantly altered in abundance with $p < 0.05$.

2.18. Quantitative proteomic analysis of mitochondrial proteins

40 μg of mitochondrial proteins obtained from WT and mGD were reduced, alkylated and digested as described above, with the only difference being the amount of trypsin added for digestion: 12.5 ng/μL trypsin in 50 mM ammonium bicarbonate was added to the samples with an enzyme to protein ratio of 1:50. Digested samples derived from total mitochondrial lysates were desalted, dried under vacuum and suspended in 80 μL of 3% acetonitrile (ACN)/0.1% FA. For each sample, 2 μL were injected in the LC system and separation of peptides was carried out with a linear gradient of ACN/0.1% FA from 3 to 40% in 40 min using the same acquisition method described above. Two technical replicates were acquired for each sample. Processing of raw files, filtering, and quantitative analysis were performed as detailed above. Data were normalized on the median to correct for possible technical variations between different LC-MS/MS analyses.

2.19. Thioredoxin reductase activity

For the estimation of the total TrxR activity in cytosolic or mitochondrial lysates, aliquots (50 μg proteins) were added to 0.2 M NaKPi buffer (pH 7.4), 5 mM EDTA, and 2 mM DTNB in a final volume of 250 μL. After 2 min, the reaction was started with 0.4 mM NADPH and DTNB reduction was followed spectrophotometrically at 412 nm for 10 min.

2.20. Glutathione reductase activity

In cytosolic and mitochondrial lysates, glutathione reductase (GR) specific activity was estimated on 50 μg of proteins and measured in 0.2 M Tris-HCl buffer (pH 8.1), 1 mM EDTA and 0.25 mM NADPH. The assay was started by the addition of 1 mM oxidized glutathione (GSSG) and NADPH consumption was measured spectrophotometrically at 340 nm.

2.21. Glutaredoxin activity

The standard assay for Grx2 activity relies on the procedure developed by Mieyal et al. [25] as modified by Raghavachari and Lou [26]. Basically, the enzymatic activity was assessed at 30 °C in 0.2 M NaKPi buffer (pH 7.4), 5 mM EDTA, 0.5 mM GSH, 70 nM GR and 0.2 mM NADPH with 2 mM hydroxyethyldisulfide (HED) as Grx2 substrate on 50 μg of cytosolic or mitochondrial proteins. NADPH decrease was followed at 340 nm. To determine Grx2 activity, the slope of the linear portion of the NADPH consumption curve was utilized.

2.22. Hexokinase activity

Hexokinase activity was measured as previously described [27]. Briefly, liver was lysed in 50 mM Tris-HCl, pH 7.5, 1 mM EDTA, 150 mM NaCl, 1% NP-40, 1 mM DTT, protease inhibitor cocktail, and incubated for 30 min at 4 °C. 40 μg of total proteins were mixed with the reaction buffer (50 mM Tris-HCl, pH 7.5, 10 mM $MgCl_2$, 0.6 mM ATP, 100 mM glucose, 0.2 mM $NADP^+$ and 0.1 units of glucose-6-phosphate dehydrogenase per mL). The absorbance at 340 nm was estimated with a plate reader every 15 s for 15 min. Enzyme activity was calculated as the change in absorbance/min in the linear portion of the curve.

2.23. Aconitase activity

Aconitase activity was assessed as previously reported [28]. Briefly, mitochondrial lysates (10 and 20 μg protein) were loaded on an aconitase activity gel constituted by a stacking gel (4% acrylamide, 67 mM Tris, 67 mM borate and 3.6 mM citrate) and a running gel (8% acrylamide, 132 mM Tris, 132 mM borate and 3.6 mM citrate). Electrophoresis was carried out at 170 V with a specific running buffer (25 mM Tris, 192 mM glycine and 3.6 mM citrate, pH 8.3). Aconitase activity was measured by incubating the gel in 100 mM Tris (pH 8.0), 1 mM $NADP^+$, 2.5 mM *cis*-aconitic acid, 5 mM $MgCl_2$, 1.2 mM 3-(4,5-dimethylthiazol-2-yl)-2,5-diphenyltetrazolium bromide, 0.3 mM phenazine methosulfate, and 5 units/mL isocitrate dehydrogenase from bovine heart (Boeringher Ingelheim, Ingelheim am Rhein, Germany) for 1 h in the dark at 37 °C. Quantitation of the gel bands was performed using ImageJ software.

2.24. Measurement of mice and food weight

Mice (1 and 6 months of age) were kept in the same groups as they were housed and the food was weighted once a week at the same time of the day following the schedule of the animal facility routines before the cage change, to not cause any stress conditions to the animals. For the body weight, WT and mGD mice ($n \geq 5$) were weighted from 8 weeks of age every other week until 44 weeks of age.

2.25. Glucose tolerance test

3 months-old WT and mGD mice were subjected to the Intraperitoneal Glucose Tolerance Test. Briefly, 3 days before the test, the animals were trained to human handling to avoid stress and adrenaline release during the test. After 12h starving, animals were weighted and the initial glycemic level was checked using Roche/Accu-chek glucose strips. Immediately after 2 mg glucose/g of mouse were injected intraperitoneally with a 27G needle. A drop of blood was collected from the tail and the glucose level measured at different time points.

2.26. Primary hepatocytes isolation

Mice were sacrificed and the liver was perfused, through a needle aligned along the inferior vena cava, with Hank's Balanced Salt Solution and Liver digest medium (Sigma-Aldrich, St. Louis, MO, USA). The perfused liver was then dissected, suspended in liver digest medium and filtered through 70 μm cell strainer to remove connective tissue debris and cell clumps. Hepatocytes were centrifuged (420×*g*, 5 min at room temperature), the pellet was suspended in plating medium (DMEM, high glucose Gibco 31966 supplemented with 10% FBS, pen/strep, 1 μM dexamethasone, 0.1 μM insulin) plus 10% Percoll solution in PBS (1:1) and centrifuged at 420×*g* for 5 min at room temperature. Cell viability, measured by trypan blue exclusion, was more than 85%.

2.27. Quantifications of total cholesterol, triglycerides and free fatty acids in mouse plasma

WT and mGD mice of 1 and 3 months of age were sacrificed, and their blood collected in 0.45 M EDTA-treated tubes. Cells were removed from plasma by centrifugation at 2000×*g* for 15 min at 18 °C. A second centrifugation at 2000×*g* for 15 min was performed to remove platelets from the sample. The resulting supernatant is the plasma utilized for the subsequent lipid quantifications. If not immediately used, plasma was stored at −80 °C. 10 μL of each sample were used for total cholesterol (Cholesterol CP, ABX Pentra, cod. A11A01634) and triglycerides (Triglycerides CP, ABX Pentra, cod. A11A01640) evaluation, which was performed in duplicate according to manufacturer's instruction. A 4-fold dilution was performed on plasma for free fatty acid (C8 and longer) estimation (Free Fatty Acid Quantitation Kit, Sigma-Aldrich, cod. MAK044), according to manufacturer's instruction. The colorimetric products by enzymatic reactions were monitored at 570 nm with Victor Nivo spectrophotometer (PerkinElmer, Waltham, MA, USA). Limit of detection for total cholesterol assay was 0.09 mmol/L (3.48 mg/mL), whilst intra- and inter-assay accuracies were 0.65% and 2.7%, respectively. Limit of detection for triglycerides assay was 0.08 mmol/L (7 mg/mL), while intra- and inter-assay accuracies were 1.5% and 1.63%, respectively.

2.28. Statistical analysis

Statistical analysis was performed using Instat software (GraphPad Software, Dan Diego, CA, USA). An unpaired *t*-test was used to identify differences between two groups, while one-way ANOVA followed by Tukey test was used to detect differences between several groups. A p value < 0.05 was considered significant. For the proteomic analysis see paragraph 17 and 18 of Materials and methods.

All results reported are the mean ± SD. The numerosity for each experiment is indicated in the figure captions.

3. Results

3.1. Characterization of the mGD mouse model

The whole-body mitochondrial Grx2 depleted (mGD) mouse model was generated by targeting exons 1c, 1a and 2 of murine *Glrx2* gene in a C57BL/6J background and replacing them by a Neomycin cassette which was subsequently excised (Fig. 1a and ref [29]. We validated the genetic modification by PCR analysis. Grx2 expressed in mGD mice lacks exon 1 and includes exon 3 (where the active site is located) and exon 4 in all the organs tested (Fig. 1b and S1a). To demonstrate that Grx2 was absent in mGD mouse mitochondria, we carried out both an immuno-gold staining for the protein of interest (Fig. 1c and c′) and a Western blot analysis (Fig. 1d and d′) in liver sections of WT and mGD mice. Grx2 protein expression was limited to the cytosolic compartment as no Grx2 was detected inside mitochondria in mGD mice. Immuno-gold staining negative controls were also performed by incubating the section with the sole secondary antibody with no spurious reactivity observed (Fig. S1b). Other organs (heart, brain, and kidney) were also tested for the protein expression and all of them showed a depletion of Grx2 in the mitochondrial fraction (Fig. S1c and c′). Altogether, these results corroborate the occurrence of the whole-body mitochondrial depletion of Grx2a in mGD mice.

3.2. Effects of Grx2 mitochondrial deficiency on metabolic parameters

The mGD mice developed and reproduced normally, and their lifespan was comparable to that of WT animals. However, we observed a significant increase in body weight with respect to WT mice starting from the 20th week of age (Fig. 2a). The food provided to the cages was weighted every 7 days as described, but no differences in food consumption was seen as compared to WT mice both at 1 and 6 months of age (Fig. 2b). With the aim of studying possible early alterations, we measured the plasma lipid levels of 1 and 3 months-old animals, a few weeks before they started to become overweight. Compared to WT animals, mGD mice showed an early rise in total cholesterol in the circulation at 1 month of age (Fig. 2c), followed by an increase in plasma levels of triglycerides (Fig. 2d) and free fatty acids (Fig. 2e) at 3 months of age. Total cholesterol and triglycerides levels were analyzed also in fasted 3 months-old mice and both parameters were significantly increased in mGD animals with respect to the WT (Fig. S2). This early hyperlipidemia, index of a metabolic phenotype, prompted us to do further investigations. The livers of 3-months-old mGD animals displayed a significantly enlarged morphology and had a whitish appearance, possibly indicating an increase in lipid accumulation (Fig. 2f). To confirm this observation, Oil Red O (ORO) staining which selectively marks lipids, and transmission electron microscope (TEM) analysis of the liver sections were performed. As shown in Fig. 2g and g′, a larger amount of lipids was accumulated in the mGD liver sections with respect to the WT (shown as increased red staining of lipids in mGD hepatic sections). Accordingly, the observation of the ultrathin sections at the TEM, confirmed a significant increase in number of lipid droplets (white dots marked with red arrows) in the cytosol of the mGD hepatocytes (Fig. 2h and h′). This phenotype is referred to as hepatic steatosis or fatty liver and is associated with an altered metabolic status.

In summary, mGD mice became overweight with aging and displayed an early onset of fatty liver and an increase in plasma lipid content, suggesting the possible occurrence of MAFLD.

3.3. Grx2 deficiency affects the expression of genes involved in lipid metabolism

Based on the metabolic phenotype involving lipid handling, we investigated the mRNA expression of genes engaged in lipid synthesis, uptake, degradation and transport in 1 and 3 months-old livers, with a major focus on genes previously correlated with MAFLD in patients [30]. The hepatic mRNA expression of the genes involved in cholesterol and fatty acids metabolism in mGD livers with respect to the WT is shown in Fig. 3a and a′ (fed mice) and 3b and b′ (fasted animals), respectively. The relative raw data are reported in Fig. S3 in Supplementary material. Regarding cholesterol metabolism, we first considered *Cyp7a1* encoding for Cytochrome P-450 7a1 which is expressed

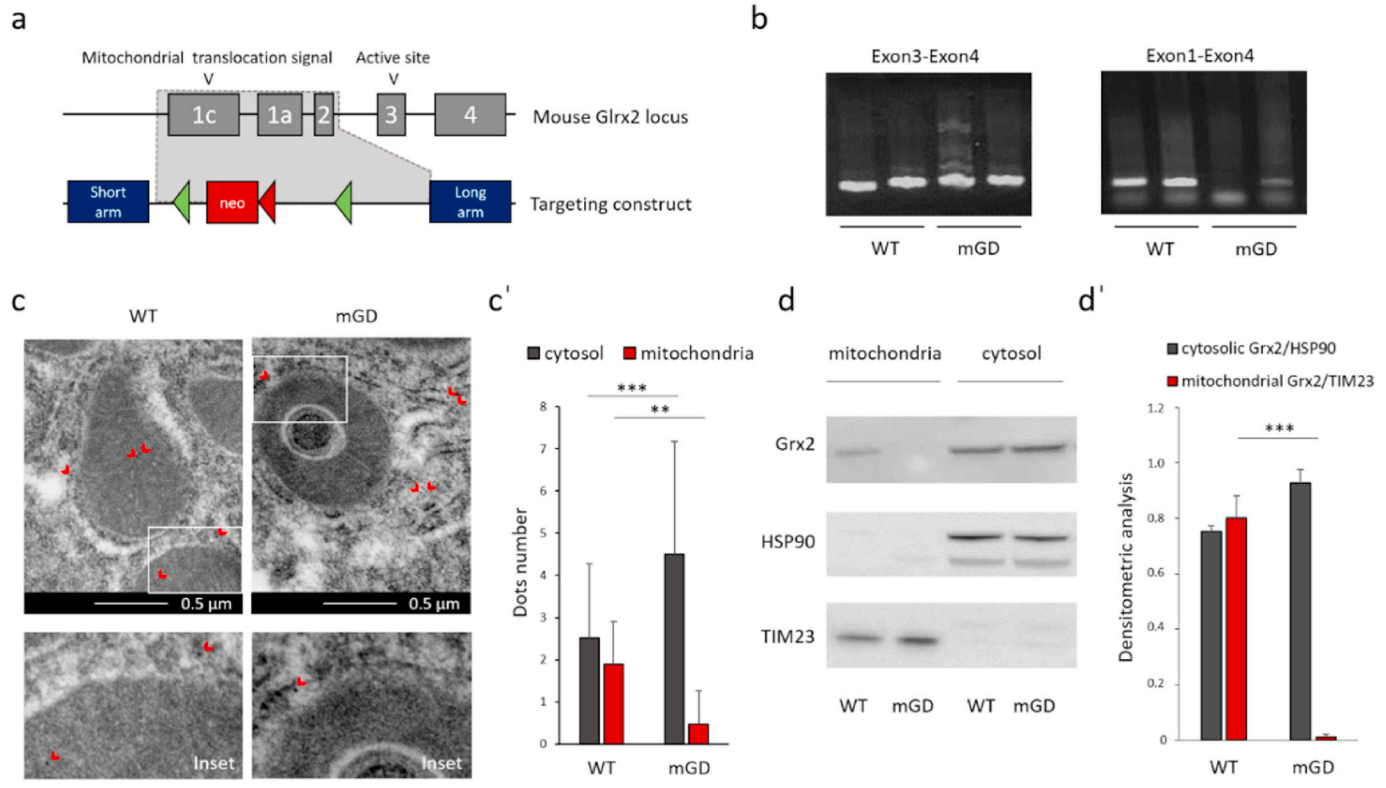

Fig. 1. Characterization of the mGD mouse model. a) Genomic structure and a partial restriction map of the mouse Grx2 locus. **b)** PCR amplification to check expression of the different exons of Grx2 in the liver tissue of WT and mGD mice (Exon3Fwd-Exon4Rev and Exon1Fwd-Exon4Rev). **c)** Representative images of the immunogold labelling of Grx2 in liver sections from WT and mGD mice. **c′)** Number of gold dots per field observed in **c** inside or outside mitochondria as the mean ± SD of 30 fields for each genotype analyzed using ImageJ software. Mean ± SD of 2 experiments (N = 4, **p < 0.01, ***p < 0.001). **d)** Western blot analysis of Grx2 expression in the liver mitochondrial fractions; HSP90 and TIM23 are utilized as markers of the cytosolic and mitochondrial fractions, respectively. **d′)** Densitometric analysis of the Western blot bands reported in **d** performed using ImageJ software using HSP90 and TIM23 as loading controls for the cytosolic and the mitochondrial fractions, respectively. Mean ± SD of 3 experiments (N = 6, ***p < 0.001). (For interpretation of the references to color in this figure legend, the reader is referred to the Web version of this article.)

only in the liver and is responsible for decreasing cholesterol by catalyzing the rate-limiting step in bile acid biosynthesis. As shown in Fig. 3a and b, *Cyp7a1* was significantly down-regulated in mGD mice independently from their age and nutritional status. Accordingly, Low-density lipoproteins receptor (*Ldlr*) was downregulated in both ages and feeding conditions (Fig. 3 a and b). These results are of particular interest since down-regulation of *CYP7A1* and *LDLR* was also reported in MAFLD patients [31]. The expression of 3-hydroxy-3-methyl-glutaryl--coenzyme A reductase (*Hmgcr)* showed instead a biphasic trend, with an increase in 1-month-old mice and a down-regulation in 3 months-old mGD liver samples, both in fed and fasted conditions (Fig. 3a and b). These results were in accordance with the measured plasma cholesterol levels that were particularly augmented in 1 month-old animals (Fig. 2c). Furthermore, we checked the expression of Sterol regulatory element binding transcription factor 2 (*Srebf2*) that controls, among others, the transcription of genes involved in cholesterol synthesis [32], however no clear tendency was observed with respect to the WT (Fig. 3 a and b).

Then, genes associated with fatty acids metabolism were analyzed. As shown in Fig. 3a' (fed mice) and b' (fasted mice), mGD liver expressed significantly lower levels of a majority of the genes involved in the fatty acid metabolism at 3 months of age especially in fed condition, while the expression pattern of the 1 month-old mice displayed a more complex profile without a clear association with specific pathways.

Due to previous reports about cardiac phenotype in total Grx2 KO mice [33,34], the mRNA expression of the same genes was here also investigated in the heart (Fig. S4a-b′). However, the expression profile of the heart appeared to be less altered with respect to the WT, in agreement with the observed greater sensitivity of the liver with Grx2a deficiency.

These gene expression data suggest that mGD mice recapitulate hepatic alterations previously associated with the development of fatty liver and MAFLD in humans. The expression of other genes related to lipid metabolism was also explored and reported in Fig. S4 c and c′. Moreover, our data underlines the importance of characterizing the gene expression both during fed and fasting conditions because expression levels of metabolic genes are dependent on the nutritional status of the animal.

Since MAFLD is often associated with an increase in inflammation, we analyzed the expression of different markers of inflammation. However, we did not detect any greater expression of these markers in mGD liver in comparison to WT organs, neither in fasting nor in fed conditions (Fig. S5). These findings indicate that this pathway is not involved in the pathogenesis of mGD phenotype. Taken together, our data point out that, in the liver, the lack of Grx2 in mitochondria affects mainly cholesterol metabolism and the expression of genes previously associated with MAFLD.

3.4. *Effects of Grx2 deficiency on mitochondrial bioenergetic functions*

To study the role of Grx2 in mitochondria, we analyzed the morphology and functionality of isolated liver mitochondria of 3 months-old WT and mGD animals. TEM morphological analysis of isolated mouse liver mitochondria (MLM) led to several interesting observations. In particular, mGD MLM showed an altered conformation with respect to the WT with the outer membrane stretched and

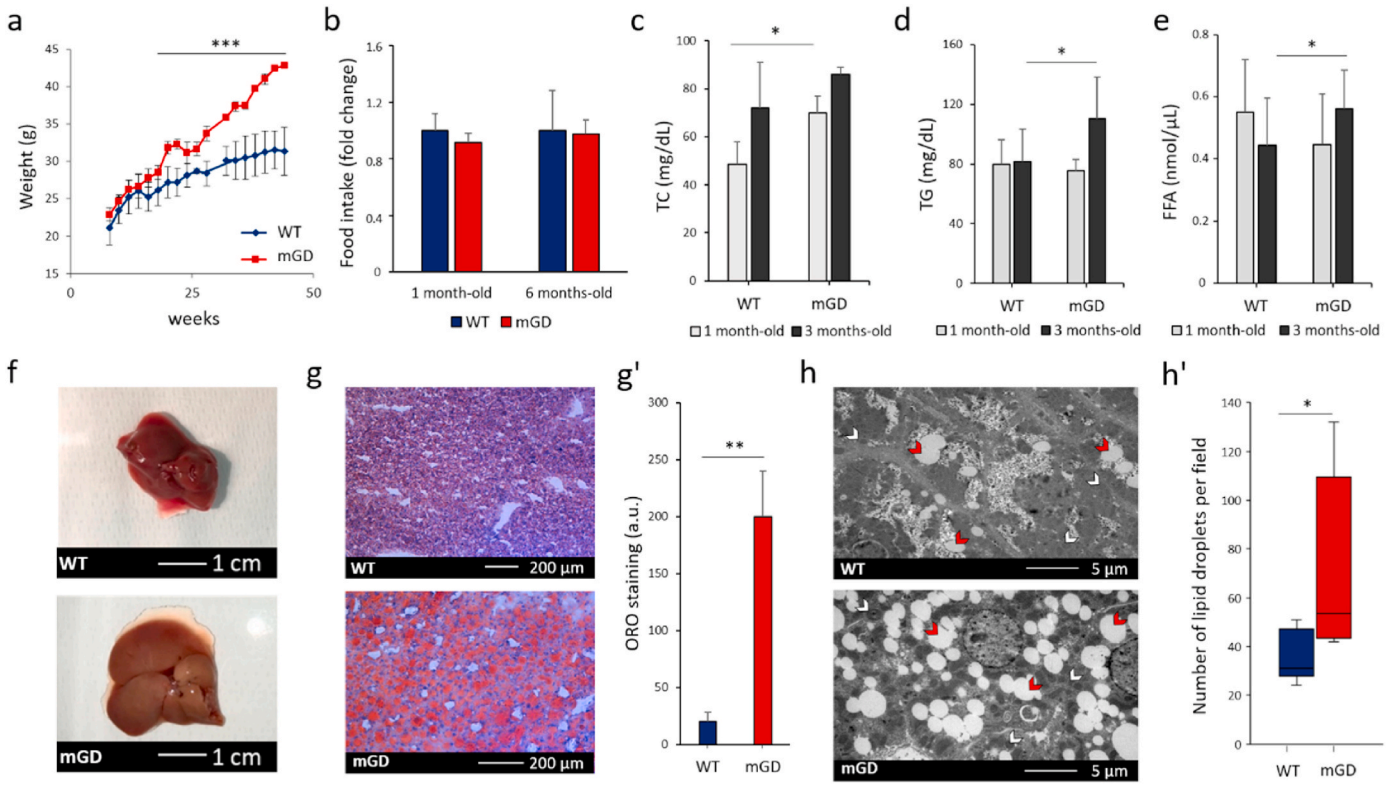

Fig. 2. Influence of Grx2 mitochondrial deficiency on metabolic parameters. **a)** Body weight curves of WT and mGD mice (N = 5, ***p < 0.001). **b)** Relative food intake of mGD mice with respect to the WT (N WT = 6, 8; N mGD = 4, 8 *p < 0.05). **c)** Total cholesterol levels measured in plasma of fed WT and mGD mice at 1 and 3 months of age (N = 6, *p < 0.05). **d)** Plasma triglyceride levels assessed in fed WT and mGD mice at 1 and 3 months of age (N = 6, *p < 0.05). **e)** Free fatty acid levels determined in plasma of 1 and 3 months-old fed WT and mGD mice (N = 6,*p < 0.05). **f)** Representative picture of livers from mGD and WT mice at 3 months of age. **g)** Representative images of the ORO/hematoxylin histological staining of WT and mGD liver sections. **g')** ORO staining quantification of 10 fields for each genotype using ImageJ software. Mean ± SD of 3 experiments (N = 6, **p < 0.01). **h)** Representative TEM images of WT and mGD liver sections. Red arrows indicate lipid droplets; white arrows point out mitochondria. **h')** Number of lipid droplets observed per field as the mean ± SD of 30 images for each genotype analyzed using ImageJ software. Mean ± SD of 3 experiments (N = 6, ***p < 0.001). (For interpretation of the references to color in this figure legend, the reader is referred to the Web version of this article.)

presenting blebs, the inner membrane curled up and collapsed creating structures with a "c" or donut shape and a more electron-dense mitochondrial matrix (Fig. 4a). This feature was not due to the isolation process, since these alterations were also observed in liver sections (Fig. S6a). Next, we performed the swelling assay as a first assessment of mitochondrial functional integrity. As reported in Fig. 4b, purified WT MLM appeared as a homogeneous population and, in the presence of succinate as respiratory substrate, maintained their light scattering level for the whole duration of the assay. In addition, WT MLM showed a classical response with about 40% of swollen mitochondria after 15 min, in the presence of 40 µM calcium chloride. On the contrary, mGD MLM displayed a noticeable population of swollen mitochondria already in basal conditions, a feature exacerbated by the addition of calcium ions (40 µM calcium chloride), leading to the swelling of the entire mitochondrial population after 15 min (Fig. 4b). These results indicate an increased sensitivity of mGD MLM towards mitochondrial permeability transition and an increased susceptibility to mitochondrial depolarization in the mGD, suggesting mitochondrial impairment.

This analysis led us to investigate specific mitochondrial parameters such as mitochondrial membrane potential and mitochondrial respiration. The mitochondrial membrane potential of WT and mGD MLM was assessed using rhodamine 123 dye, as described in the Material and methods section. Fig. 4c shows the experimental results as a ratio between the fluorescence measured before and after addition of the substrate and expressed as percentage with respect to WT MLM in the presence of EGTA, taken as control of the maximum membrane potential reached. An example of raw measurements is shown in Fig. S6b. As displayed in Fig. 4c, in accordance with the swelling assay, in basal conditions mGD MLM exhibited, after energization with succinate, a limited decrease of the probe fluorescence, indicating a lower capacity of mGD MLM to establish a mitochondrial membrane potential with respect to the WT. However, in the presence of a calcium chelator (20 µM EGTA) or of an inhibitor of the mitochondrial membrane permeability transition (1 µM cyclosporin A), the membrane potential of mGD MLM was similar to the WT. Moreover, the addition of increasing concentrations of calcium ions determined a more pronounced and rapid rise of the fluorescence intensity in mGD MLM as compared to WT in all the conditions tested (Fig. 4c and S6b), indicating a decrease of the mitochondrial transmembrane potential and showing an enhanced calcium sensitivity of mGD mitochondria. In addition, a lower mitochondrial membrane potential of mGD MLM was also observed using the substrate palmitoylcarnitine (Fig. S6c) which fuels the β-oxidation pathway, indicating that the observed decrease in mitochondrial membrane potential seen was independent from the substrate used.

Then, mitochondrial energetics was evaluated comparing the oxygen consumption rate of mGD and WT MLM. Remarkably, a significant lower rate of ADP-stimulated respiration was observed in mGD MLM in the presence of glutamate plus malate (Glu/Mal) as oxidizable substrates (Fig. 4d). Similarly, uncoupled respiration was lower in mGD MLM in comparison to the WT. On the other hand, when succinate (Succ) was employed as substrate to boost respiration, an increase in oxygen consumption rate was observed in state 4 of mGD MLM (Fig. 4d') but showing lower values of O_2 consumption after ADP or FCCP addition in comparison to WT MLM, indicating a potential uncoupled state already

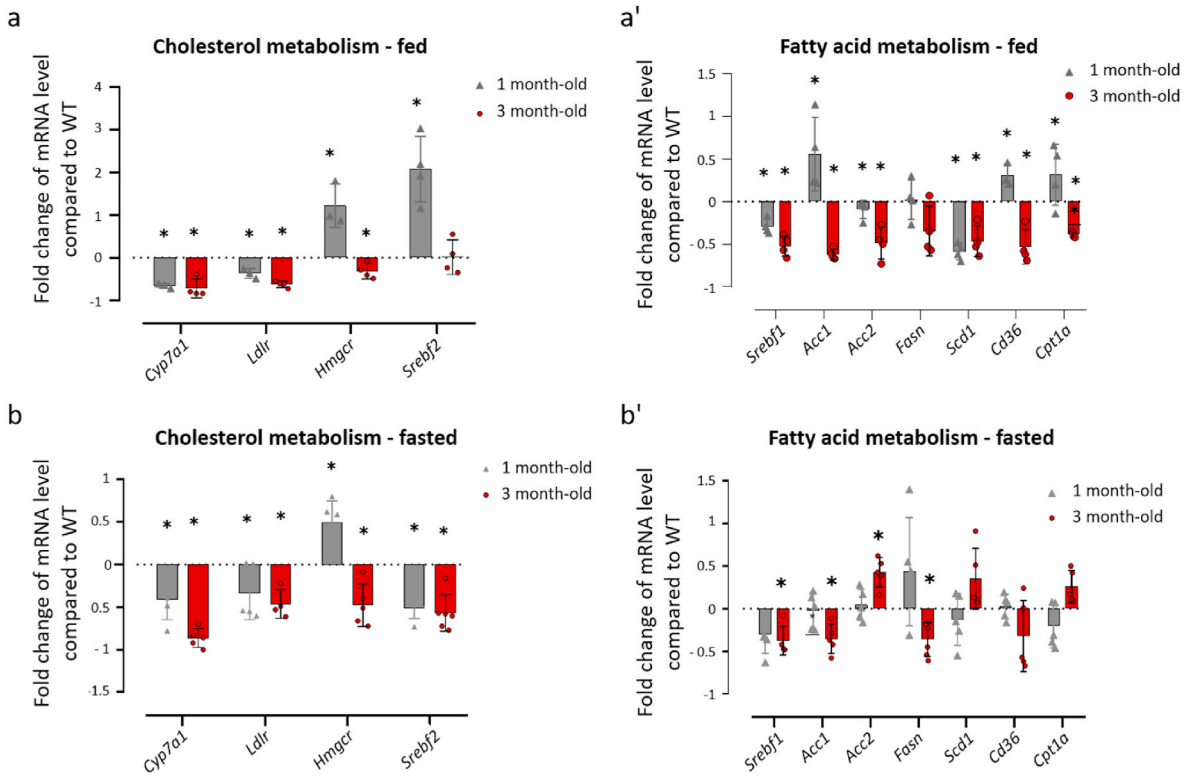

Fig. 3. Expression of genes of cholesterol and fatty acid metabolism in WT and mGD livers. mRNA expression of genes involved in lipid metabolism assessed via RT-qPCR in the liver of fed animals **(a, a')** and of fasted mice **(b, b')**. Mean ± SD of 3 experiments (N ≥ 4) is shown (*p < 0.05). *Cyp1a7*: Cytochrome P-450 7a1; *Ldlr*: LDL receptor; *Hmgcr*: 3-hydroxy-3-methylglutaryl-CoA reductase; *Srebf1-2*: Sterol regulatory element-binding protein 1 and 2; *Acc1-2*: Acetyl-CoA carboxylase 1 and 2; *Fasn*: Fatty acid synthase; *Scd1*: Stearoyl-CoA desaturase; *Cd36*: fatty acid translocase *Cpt1a*: Carnitine palmitoyltransferase 1a.

in basal conditions. In fact, the determination of the respiratory control indices (state 3/state 4) confirmed a decreased respiratory capacity of mGD MLM using both substrates (Fig. 4e).

Considering these results, we also determined the oxygen consumption of MLM in the presence of palmitoylcarnitine (Fig. S6d). With this alternative substrate which feeds the mitochondrial β-oxidation, the rate of oxygen consumption is slower than that with direct TCA cycle substrates in both genotypes but, also in this case, the respiratory capacity of mGD MLM was lower in comparison to WT MLM (Fig. S6d).

Altogether, these results point out that mGD MLM have a decreased mitochondrial activity as revealed by their membrane potential, oxygen consumption rates and an increased sensitivity to mitochondrial permeability transition, especially in the presence of calcium ions.

The observation that mitochondrial respiration was particularly affected when Glu/Mal were used as substrates implies a major impairment of complex I of the electron transport chain (ETC). For this reason, we analyzed the mitochondrial proteome of mGD liver mitochondria to assess possible differences in the abundance of specific proteins. As reported in Table 4 some key clusters of proteins were identified to be both down- and up-regulated in mGD MLM (complete results of this proteomic analysis are reported in Table S1). As expected regarding the downregulated genes, various subunits of complex I were less abundant in mGD MLM in accordance with a lower Glu/Mal induced respiration. Some constituents of Complex III and IV were also downregulated suggesting that Grx2 depletion impinges on other components of the ETC. Furthermore, some enzymes involved in the tricarboxylic acid (TCA) cycle showed a moderate reduction of abundance in KO mice. To check whether this lowered expression was associated with a decrease in TCA cycle function itself, we measured aconitase activity which indeed was found to be slightly reduced in mGD MLM samples (Fig. S6e). In addition, some proteins involved in cristae formation were also less abundant in mGD mitochondria which correlated with the altered organelle morphology described previously (Fig. 4a). On the contrary, the mitochondrial proteins which displayed an increased abundance in mGD MLM are mainly involved in steroid hormones biosynthesis and fatty acid β-oxidation.

3.5. *mGD liver mitochondria display an altered redox signaling*

Considering the known functions of Grx2, it is important to assess the effect of Grx2 depletion on the redox signaling and iron handling capacity of mGD mitochondria. Indeed, the proteomic analysis revealed a reduced abundance of several iron-sulfur proteins in mGD MLM (Table 4). Fig. 5a shows the amount of protein-bound iron as detected by atomic absorption analysis in liver mitochondria obtained from the two genotypes. mGD MLM displayed a lower incorporation of iron as prosthetic group into mitochondrial proteins, confirming a role of Grx2a in the managing of iron-sulfur clusters. Iron is a redox active metal, which also can promote an imbalance in redox homeostasis. However, when we analyzed the concentration of total glutathione and its oxidized form, no significant differences were detected between WT and mGD liver mitochondria (Fig. 5b), although the levels of total thiols exhibited a slight but not significant decrease (Fig. 5c). Other organs were also tested for their thiols and glutathione level with no major variations found (Figs. S7a and b). However, lipid infiltration was also observed in the heart (Fig. S7c). These data led us to conclude that the redox environment in the mitochondrial compartment does not appear to be heavily affected in mGD MLM, even though an altered redox signaling involving the reactive cysteines could be envisaged. Thus, using AmplexRed probe, we monitored H_2O_2 production from isolated mGD and WT liver mitochondria. As shown in Fig. 5d and d′, an increased basal ROS production was observed in mGD compared to WT MLM. Moreover, in the presence of 1 μM CsA, a known inhibitor of the permeability transition pore, mGD MLM still produced more ROS than

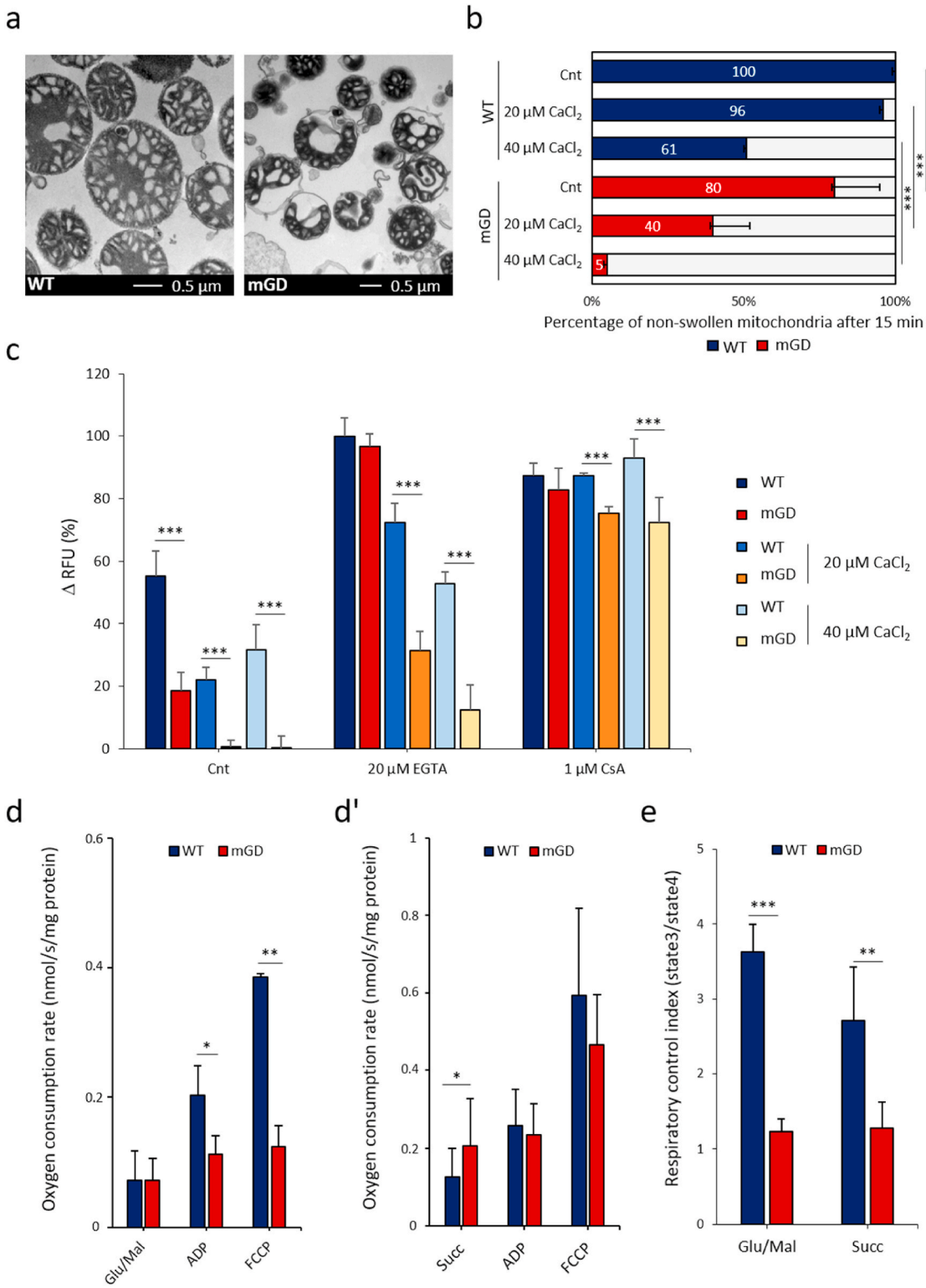

Fig. 4. Effects of Grx2 deficiency on mitochondrial functions. a) Representative TEM images of a standard preparation of WT and mGD liver mitochondria. **b)** Effect of Ca^{2+} ions on WT and mGD mitochondrial swelling reported as percentage of swollen or non-swollen mitochondria using succinate as substrate. Mean ± SD of 6 experiments (N = 18, ***$p < 0.001$). **c)** Mitochondrial membrane potential of WT and mGD MLM referred as percentage of the maximum Δ value of relative fluorescence (RFU) after 8 min from substrate addition (5 mM succinate) in the indicated conditions as described in Material and methods. Mean ± SD of 6 experiments, (N = 18, ***$p < 0.001$). **d-e)** Mitochondrial respiratory capacity of WT and mGD mouse liver mitochondria. Mean ± SD of 10 experiments, (N = 32, *$p < 0.05$, **$p < 0.01$, ***$p < 0.001$). The values of oxygen consumption rates (basal, after ADP addition and after FCCP addition) obtained in the presence of either glutamate/malate (Glu/Mal) (**d**) or succinate (Succ) (**d′**) as substrates, are shown. The respiratory control index (state 3/state 4) in the presence of the different substrates is reported in **e**.

Table 4
Proteomic analysis of mGD MLM. Proteins showing a decreased or increased in abundance in mGD with respect to the WT are reported with the respective fold-change and grouped according to their biological function.

Biological function	Gene Name	Protein Description	Fold change
ETC complex I	*Ndufa4*	*Cytochrome c oxidase subunit NDUFA4*	*- 1.3*
	Ndufa6	*NADH dehydrogenase [ubiquinone] 1 alpha subcomplex subunit 6*	*- 1.3*
	Ndufa7	*NADH dehydrogenase [ubiquinone] 1 alpha subcomplex subunit 7*	*- 1.3*
	Ndufa9	*NADH dehydrogenase [ubiquinone] 1 alpha subcomplex subunit 9, mitochondrial*	*- 1.4*
	Ndufa10	*NADH dehydrogenase [ubiquinone] 1 alpha subcomplex subunit 10, mitochondrial*	*- 1.3*
	Ndufa11	*NADH dehydrogenase [ubiquinone] 1 alpha subcomplex subunit 11*	*- 1.4*
	Ndufa12	*NADH dehydrogenase [ubiquinone] 1 alpha subcomplex subunit 12*	*- 1.2*
	Ndufa13	*NADH dehydrogenase [ubiquinone] 1 alpha subcomplex subunit 13*	*- 1.3*
	Ndufb1	*NADH dehydrogenase [ubiquinone] 1 beta subcomplex subunit 1*	*- 1.5*
	Ndufb4	*NADH dehydrogenase [ubiquinone] 1 beta subcomplex subunit 4*	*- 1.2*
	Ndufb9	*NADH dehydrogenase [ubiquinone] 1 beta subcomplex subunit 9*	*- 1.6*
	Ndufv1	*NADH dehydrogenase [ubiquinone] flavoprotein 1, mitochondrial*	*- 1.3*
	Ndufv2	*NADH dehydrogenase [ubiquinone] flavoprotein 2, mitochondrial*	*- 1.2*
	Ndufs3	*NADH dehydrogenase [ubiquinone] iron-sulfur protein 3, mitochondrial*	*- 1.2*
	Ndufs7	*NADH dehydrogenase [ubiquinone] iron-sulfur protein 7, mitochondrial*	*- 1.6*
	Ndufs8	*NADH dehydrogenase [ubiquinone] iron-sulfur protein 8, mitochondrial*	*- 1.2*
ETC complex III	*Cyc1*	*Cytochrome c1, heme protein, mitochondrial*	*- 1.2*
	mtCo2	*Cytochrome c oxidase subunit 2*	*- 1.2*
	Uqcrb	*Cytochrome b-c1 complex subunit 7*	*- 1.3*
	Uqcrc1	*Cytochrome b-c1 complex subunit 1, mitochondrial*	*- 1.2*
	Uqcr10	*Cytochrome b-c1 complex subunit 9*	*- 1.6*
ETC complex IV	*Cox4i1*	*Cytochrome c oxidase subunit 4 isoform 1, mitochondrial*	*- 1.2*
	Cox6a1	*Cytochrome c oxidase subunit 6A1, mitochondrial*	*- 2.2*
	Cox6b1	*Cytochrome c oxidase subunit 6B1*	*- 1.4*
	Cox6c	*Cytochrome c oxidase subunit 6C*	*- 1.4*
TCA cycle	*Dld*	*Dihydrolipoyl dehydrogenase, mitochondrial*	*- 1.2*
	Idh3a	*Isocitrate dehydrogenase [NAD] subunit alpha, mitochondrial*	*- 1.2*
	Ogdh	*2-oxoglutarate dehydrogenase, mitochondrial*	*- 1.3*
	Sdha	*Succinate dehydrogenase [ubiquinone] flavoprotein subunit, mitochondrial*	*- 1.2*
	Sucla2	*Succinate–CoA ligase [ADP-forming] subunit beta, mitochondrial*	*- 1.3*
	Suclg1	*Succinate–CoA ligase [ADP/GDP-forming] subunit alpha, mitochondrial*	*- 1.4*
Sulfur metabolism	*Cisd3*	*CDGSH iron-sulfur domain-containing protein 3, mitochondrial*	*- 2.7*
	Ethe1	*Persulfide dioxygenase ETHE1, mitochondrial*	*- 1.4*
	Mpst	*3-mercaptopyruvate sulfurtransferase*	*- 1.5*
	Sqor	*Sulfide:quinone oxidoreductase, mitochondrial*	*- 2.3*
Cristae formation	*Chchd3*	*MICOS complex subunit*	*- 1.4*
	Immt	*MICOS complex subunit MIC60*	*- 1.2*
	Letm1	*Mitochondrial proton/calcium exchanger protein*	*- 1.3*
	Samm50	*Sorting and assembly machinery component 50 homolog*	*- 1.3*
Steroid hormones biosynthesis	*Cyp2d26*	*Cytochrome P450 2D26*	*+ 2.3*
	Cyp2e1	*4-nitrophenol 2-hydroxylase*	*+ 1.5*
	Cyp3a11	*Cytochrome P450 3A11*	*+ 1.6*
	Cyp4a10	*Cytochrome P450 4A10*	*+ 8.9*
	Cyp4a14	*Cytochrome P450 4A14*	*+ 10.7*
	Cyp4v2	*Cytochrome P450 4V2*	*+ 2.0*
	Hsd3b5	*NADPH-dependent 3-keto-steroid reductase Hsd3b5*	*+ 1.4*
	Hsd11b1	*Corticosteroid 11-beta-dehydrogenase isozyme 1*	*+ 1.3*
	Ugt1a1	*UDP-glucuronosyltransferase 1A1*	*+ 1.3*
	Ugt1a5	*UDP-glucuronosyltransferase 1A5*	*+ 1.4*
	Ugt1a6b	*UDP-glucuronosyltransferase 1A6B*	*+ 1.4*
	Ugt1a9	*UDP-glucuronosyltransferase 1A9*	*+ 1.5*
	Ugt2b1	*UDP-glucuronosyltransferase 2B1*	*+ 2.0*
	Ugt2b5	*UDP-glucuronosyltransferase 2B5*	*+ 1.3*
	Ugt2b34	*UDP-glucuronosyltransferase 2B34*	*+ 1.3*
Fatty acid β-oxidation	*Abcd3*	*ATP-binding cassette sub-family D member 3*	*+ 1.8*
	Acad11	*Acyl-CoA dehydrogenase family member 11*	*+ 2.0*
	Acadvl	*Very long-chain specific acyl-CoA dehydrogenase, mitochondrial*	*+ 1.2*
	Acsl5	*Long-chain-fatty-acid–CoA ligase 5*	*+ 1.7*
	Ech1	*Delta(3,5)-Delta(2,4)-dienoyl-CoA isomerase, mitochondrial*	*+ 1.3*
	Scp2	*Non-specific lipid-transfer protein*	*+ 1.5*
	Slc27a2	*Very long-chain acyl-CoA synthetase*	*+ 1.3*

the WT. Therefore, we concluded that this significantly increase of ROS production was not dependent on the mitochondrial swelling, but was an inherent feature of mGD mitochondria. Remarkably, no significant differences in basal ROS production were detected in isolated heart mitochondria (Fig. S7d and d′) suggesting once more that the liver is more sensitive to Grx2a depletion. However, when mitochondrial complex III was inhibited by antimycin A, a significant increase of ROS was observed in mGD heart mitochondria respect to the WT (Fig. S7d and d′).

Since iron can trigger lipid peroxidation via the Fenton reaction, we quantified the lipid peroxidation of isolated MLM measured as thio-barbituric acid reactive substances (*TBARS*). Also, in this case only a slight rise in lipid peroxidation products was detected in mGD mitochondria (Fig. 5e) which, in accordance with total thiols quantifications, has a common trend towards a more pronounced state of oxidation in mGD MLM in comparison to the WT.

Regarding redox signaling we also checked whether the depletion of Grx2 in mGD MLM was balanced by a compensatory overexpression of other thiol redox enzymes. We carried out enzymatic activity assessments and Western blot analysis for various redox active enzymes present in the mitochondrial and cytosolic compartments. No alterations in the enzymatic activities of glutathione reductase and thioredoxin reductase were found in the organs tested (Fig. 5f and f′ and Figs. S7e–g). As shown in Fig. 5g and h (and relative quantifications 5g′ and h′), also the expression of redox proteins was almost identical in the two mouse genotypes from both cellular compartments suggesting that no major redox compensatory mechanisms are activated and that Grx2a probably has a peculiar function in the mitochondrial physiology.

In summary, the absence of Grx2 in mGD MLM impinges on the handling of iron-sulfur clusters, triggering ROS production and a minor increase in the overall mitochondrial oxidation, which can be associated with a modification of the redox signaling in the organelle. In addition, the amount and activity of other enzymes involved in thiol regulation

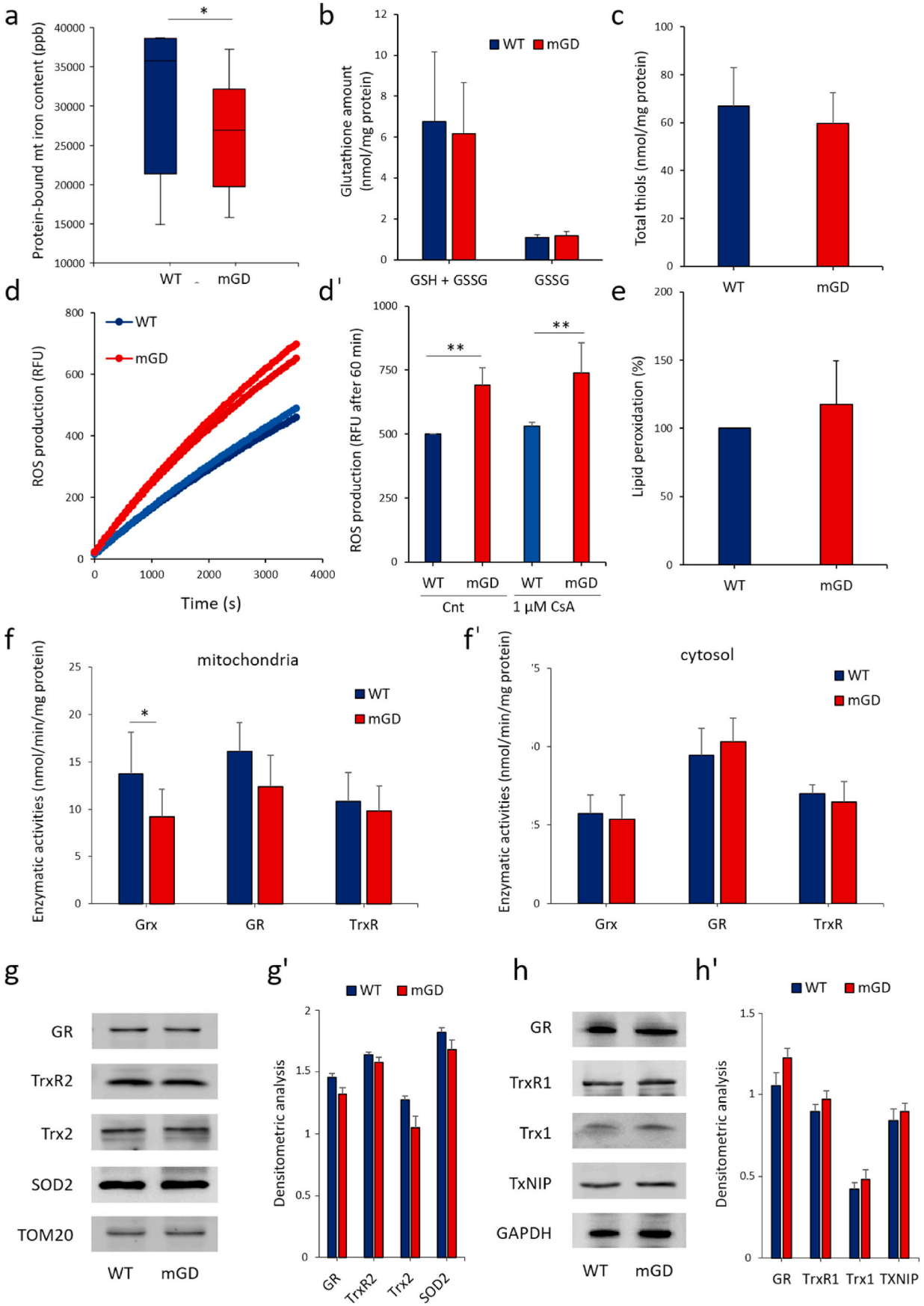

(caption on next page)

Fig. 5. Analysis of the mitochondrial redox state in WT and mGD MLM. a) Measurement of protein-bound iron in the isolated mGD and WT liver mitochondria by atomic absorption analysis. Mean ± SD of 9 experiments (N = 36, *p < 0.05). **b)** Total glutathione (GSH + GSSG) and oxidized glutathione (GSSG) content determined in isolated liver mitochondria as described in Materials and methods. Mean ± SD of 8 experiments, N = 24. **c)** Total thiols content determined in isolated liver mitochondria. Mean ± SD of 8 experiments, N = 24. **d)** ROS production of WT and mGD mouse liver mitochondria measured using the AmplexRed dye. Kinetic curves of basal or CsA-induced ROS production are reported, RFU = relative fluorescent units; CsA = cyclosporin A. **d′)** Quantification of ROS levels in WT and mGD liver mitochondria after 60 min. Mean ± SD of 5 experiments (N = 20, **p < 0.01). **e)** Lipid peroxidation (estimated as TBARS production) measured in WT and mGD MLM and expressed as percentage with respect to the WT. Mean ± SD of 4 experiments (N = 8). **f and f′)** Grx, GR and TrxR specific activities measured in the mitochondrial fraction **(f)** and cytosolic compartment **(f′)** isolated from mGD and WT livers, respectively. Mean ± SD of 12 experiments (N = 36, *p < 0.01). **g, h)** Western blot of different redox active proteins in WT and mGD liver mitochondria **(g),** or cytosol **(h)**. TOM20 and GAPDH are employed as a loading control for the mitochondrial and cytosolic fractions, respectively. **g′, h′)** Densitometric analysis of the WB shown in **g** and **h** using TOM20 or GAPDH as loading controls for the mitochondrial and cytosolic compartments, respectively. The mean ± SD of 3 experiments (N = 18) is reported.

are not affected by the absence of Grx2 suggesting a unique function of this small protein in the mitochondria.

3.6. Glucose flux is altered in mGD liver

To explore the link between the impaired liver mitochondrial activity and the metabolic phenotype observed in mGD mice, we investigated the hepatic glucose metabolism. Hexokinase 4 (HK4), also called glucokinase, plays an important regulatory role in glucose metabolism in the liver. As shown in Fig. 6a, the HK4 mRNA expression is increased in mGD liver ($p < 0.05$) of 1 month-old mice compared to the WT, confirmed by the measurement of its enzymatic activity (Fig. 6b). This difference disappears with aging and HK4 liver expression and activity becomes similar in 3 months-old mice. However, the determination of hepatic glycogen content by Periodic Acid–Schiff (PAS) staining in mice of the same age, revealed a lower accumulation of glycogen in mGD compared to WT animals (Fig. 6c).

Furthermore, we analyzed the glucose tolerance by performing an intraperitoneal glucose tolerance test (IPGTT) but we did not observe any significant difference between mGD and WT mice (Fig. 6d). Moreover, primary hepatocytes from WT and mGD mice did not show statistically significant differences in response to 100 nM insulin stimulation (Fig. 6e). Therefore, we hypothesized that the impaired glycogen storage was not due to alteration in the plasma glucose level, but more likely to a direct regulation of the pathway leading to glycogen production downstream of the insulin receptor. Upon insulin signal, Protein kinase B (AKT) phosphorylates and inactivates glycogen synthase kinase 3 β (GSK3β) blocking its inhibitory activity on glycogen synthase (GS) and allowing the synthesis of glycogen. Fig. 6f and f' report the Western blot analysis performed on WT and mGD liver cytosols for AKT and GS and their phosphorylated forms. As apparent, mGD liver displayed less AKT Ser473 phosphorylation and increased GS phosphorylation, in accordance with the lower glycogen synthesis observed in the PAS staining. For clarification, Fig. 6g shows the

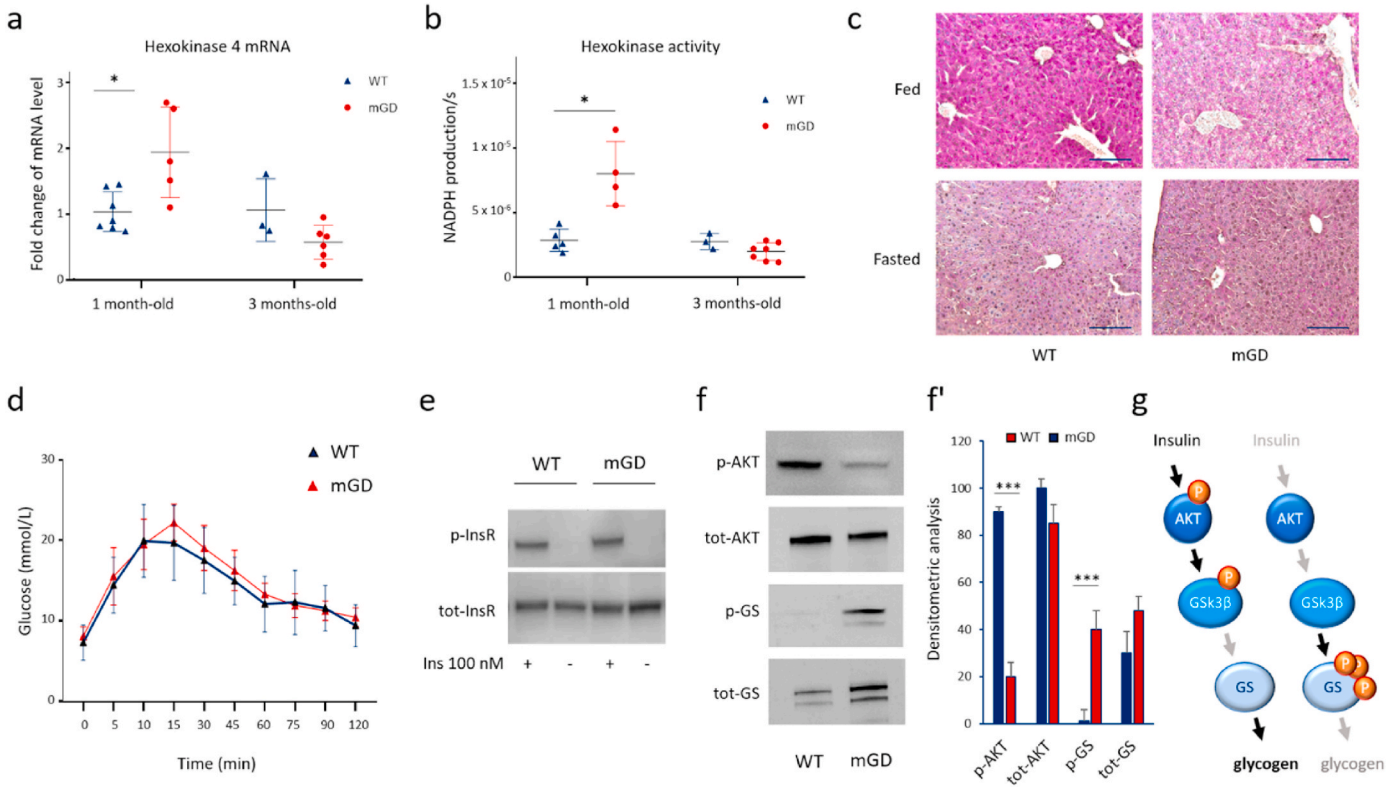

Fig. 6. Glucose metabolism evaluation in mGD mice. a, b) 1 and 3 months-old mice were sacrificed after overnight starvation and HK4 mRNA expression (**a**) and activity (**b**) were assessed. Mean ± SD of 3 experiments (N ≥ 3). **c)** Glycogen estimation via PAS staining. Representative sections of the liver from 3 months-old WT and mGD mice after overnight starvation or in fed conditions, observed with 20× objective. **d)** Glucose tolerance test of 3 months-old mice. Mean ± SD of 3 experiments (N ≥ 5). **e)** 3 months-old WT and mGD mice were sacrificed and primary hepatocytes isolated, plated and subjected to insulin stimulation. Representative results of 2 experiments (N = 6). **f)** Western blot of total AKT, *p*-AKT (Ser473), GS and p-GS (Ser641) and relative quantifications **(f')**. For the densitometric analysis the mean ± SD of 3 experiments is reported (N = 18, ***p < 0.001). **g)** Scheme of the glycogen synthesis regulatory pathway. All the experimental details are reported in Material and Methods.

phosphorylation cascade regulating glycogen synthesis. These data suggest that the observed lower production of glycogen in mGD liver was probably linked to reduced AKT phosphorylation. It has been reported that AKT dephosphorylation can be induced by ROS [35] and thus our results could indicate that the lack of Grx2 in mitochondria might promote the mitochondrial-cytosolic ROS signaling pathway, which, in turn, affects key regulators of cellular metabolism such as AKT.

3.7. Different glutathionylation pattern in mGD MLM is associated with observed phenotypic alterations

The major function of Grx2 is binding to iron-sulfur clusters as well as glutathionylation and de-glutathionylation of target proteins. We therefore investigated Grx2 dependent PTM comparing WT and mGD MLM using Western blot analysis. Interestingly, we observed a decrease

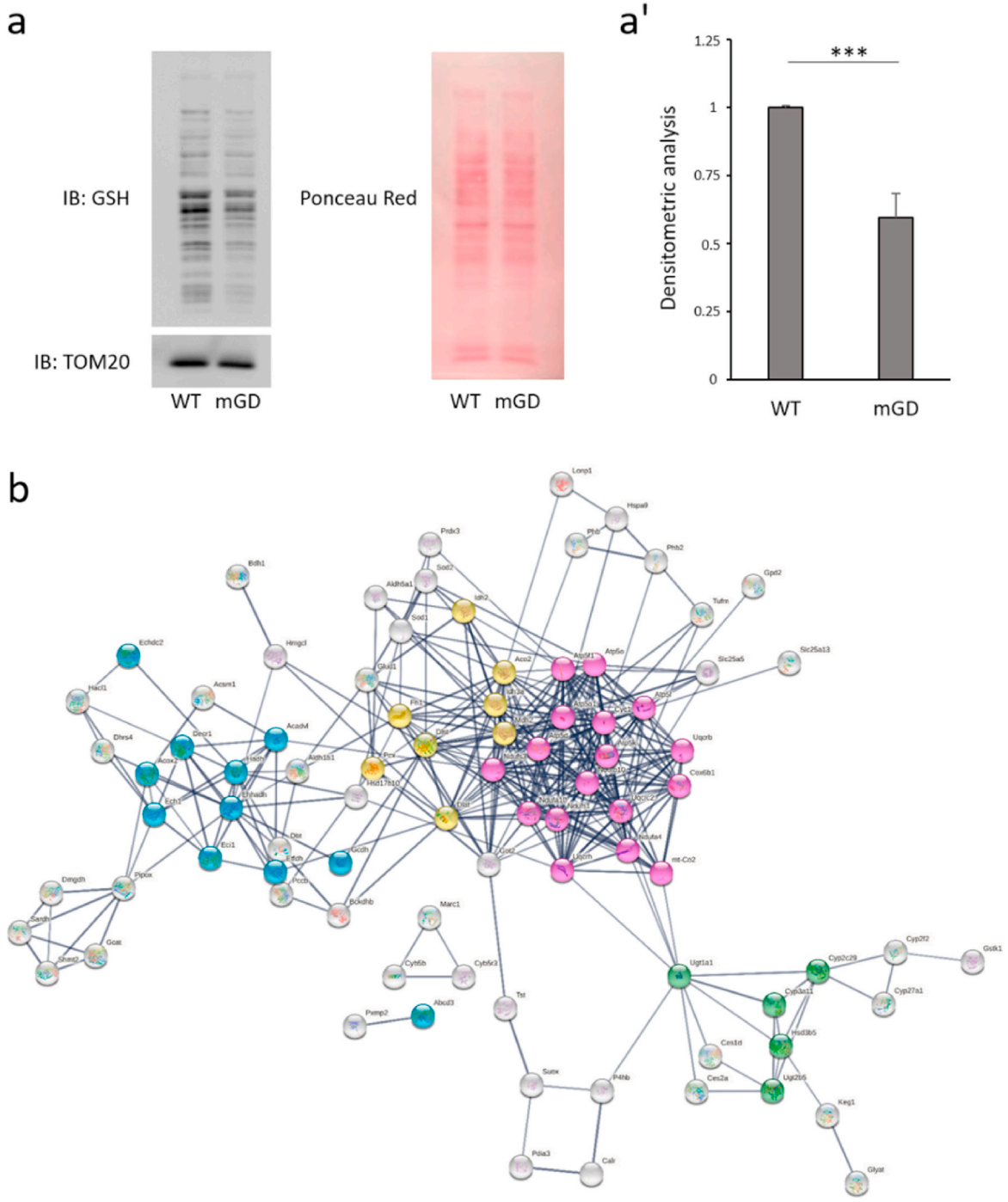

Fig. 7. Glutathionylation pattern of mitochondrial proteome in WT and mGD livers. a) Western blot of glutathionylated proteins in mice liver mitochondrial lysates with relative Ponceau red staining; **a')** Densitometric analysis of the WB in panel **a**, TOM20 is used as a loading control. Mean ± SD of 3 experiments (***$p < 0.001$). **b)** String analysis of mitochondrial proteins differentially glutathionylated in mGD with respect to WT MLM normalized on total protein abundance (high confidence 0.700). Immunoprecipitation of glutathionylated proteins was performed as described in Materials and methods, the IP proteins were identified by LC-MS/MS and normalized for the total abundance in the mitochondrial lysate. Proteins shown in the network have a fold change ≥2 or ≤ −2 between the two genotypes, with p value < 0.05. Green: Steroid hormone biosynthesis; Magenta: Oxidative phosphorylation; Yellow: TCA cycle; Light-blue: fatty acid β-oxidation. Mean ± SD of 3 experiments (N = 3) is reported. (For interpretation of the references to color in this figure legend, the reader is referred to the Web version of this article.)

in glutathionylated proteins in mGD MLM with respect to the WT (Fig. 7a and a'). To verify whether the bands observed were indeed effectively glutathionylated proteins, incubation with an *anti*-GSH antibody was performed with or without 0.1 M DTT in order to reduce GSH-mixed disulfides (Fig. 7a and S7). Therefore, we speculate that an altered mitochondrial glutathionylation might be involved in the development of the metabolic phenotype observed in mGD mice (Figs. 2 and 3). Hence, we performed a proteomic analysis of the putative glutathionylated proteins in MLM of 3 months-old mice. Liver mitochondrial lysates from WT and mGD mice were subjected to immunoprecipitation to enrich the preparation of glutathionylated proteins, as described in the Materials and methods section. A label free proteomic approach was used to obtain a relative quantification of the proteins immunoprecipitated from the different genotypes [36]. The list of all identified protein groups with a statistically significant fold change with respect to the WT samples are reported in Table S2. Useful details to assess the reliability of protein and peptide identification as well as the quantifications are included. The quantification of the putatively glutathionylated proteins were normalized based on their relative abundance as quantified from the whole mitochondrial lysate. In accordance with Fig. 7a and a', in mGD liver mitochondria, the amount of putative glutathionylated proteins was found to be lower than in WT samples, with most of the proteins showing a significant reduction in fold change (see Table S2). A String analysis [37] made using high stringency conditions (confidence set to 0.7) and shown in Fig. 7b, revealed that many of the differentially glutathionylated proteins are physically and/or functionally connected to the following pathways and biological processes: oxidative phosphorylation, TCA cycle, steroid hormone biosynthesis and fatty acid β-oxidation. Thus, the lack of Grx2 seems to affect the glutathionylation process of several metabolic enzymes present in mitochondria; for instance, the effect of Grx2 deficiency on cholesterol metabolism already observed in Fig. 3, and highlighted in the proteomic analysis of total mitochondrial proteins (Table 4), seems to be at least partially related to the altered glutathionylation of some of the enzymes involved in the pathway. The alteration in glutathionylation of some components of the respiratory complexes, together with a reduced amount of some constituents (see Table 4) may also be associated with the observed impairment of mitochondrial function reported in Fig. 4. In conclusion, the exploitation of an unbiased proteomic approach, allowed us to identify a set of mitochondrial proteins subjected to Grx2-mediated glutathionylation, suggesting that Grx2 is involved in the regulation of mitochondrial pathways associated with metabolic processes.

4. Discussion

In this study, we provide a detailed characterization of a mouse model in which the depletion of Grx2 in mitochondria leads to relevant phenotypic and metabolic changes, such as increased body weight, augmented plasma lipid levels, mitochondrial structural and functional abnormalities and altered gene expression profile that can be associated with a MAFLD phenotype.

Compared to the data published on total $Grx2^{-/-}$ mouse models [33,34], the phenotype of mGD mice is milder, indicating that the mitochondrial (Grx2a) and the cytosolic (Grx2c) variants of the enzymes have different functions; for instance the lack of Grx2a alone does not lead to heart failure as reported for the total KO mouse model [38]. A previous report by Wu et al. also described mitochondrial impairment associated with a thiol/disulfide imbalance and a significant accumulation of S-glutathionylated proteins in the lens of a total $Grx2^{-/-}$ mouse model [39]. However, the research activity was limited to the lenses of $Grx2^{-/-}$ mice which, as the authors conveyed, are particularly vulnerable to oxidation. In line with our results, Wohua and Weiming observed that, under high fat diet condition, $Grx2^{-/-}$ mice are subjected to steatotic alterations in a more pronounced way than WT animals [40]. A similar phenotype was also observed in $Grx1^{-/-}$ mice [41] but starting at later stages of life (from 8 months of age), endorsing our hypothesis of a mechanistic importance of glutaredoxins in the regulation of metabolic pathways in particular of the liver.

Grx2 plays a crucial role in the thiol redox regulation as it is at a point of convergence of the glutathione and thioredoxin systems [15,42] catalyzing both glutathionylation and deglutathionylation of proteins [1]. The role of Grx2 in this PTM is a complex issue, as Grx2 acts both as a glutathionylating and deglutathionylating agent behaving as a sensor of the GSH/GSSG redox state. Some authors [34,39] found an increased glutathionylation upon Grx2 gene deletion, suggesting that Grx2 action is directed to prevent the occurrence of oxidizing conditions. As observed by Beer et al., Grx2 can catalyze protein glutathionylation in the presence of different GSH/GSSG ratios [1]. Accordingly, Grx2 deficiency could lead to a decreased glutathionylation as apparent in our observations, indicating the occurrence of a disruption of the redox signaling in mitochondria. Therefore, we concluded that the deficiency of this enzyme determines a lack of modulation of the glutathionylation/deglutathionylation process, a condition that, with respect to the physiological state, makes protein thiols subjected to alterations relying only on the actual specific environment. In mGD mice, the absence of Grx2a leads to a decrease in glutathionylation of a specific subset of mitochondrial proteins involved in oxidative phosphorylation, steroid hormone biosynthesis, TCA cycle and fatty acid β-oxidation (Fig. 7b). In accordance with our result, Diotte et al. displayed that Grx2 overexpression increased the glutathionylation of mitochondrial proteins in mice suggesting a protective role against doxorubicin-induced cardiotoxicity and indicating a major function of Grx2 as a glutathionylating enzyme [43]. Of note, in redox homeostatic conditions, protein glutathionylation by thiol-disulfide exchange is hindered by the high intra mitochondrial GSH/GSSG ratio, prompting the requirement of an enzymatic catalysis [44] which might be performed by Grx2.

Furthermore, in our model, the absence of Grx2a, did not trigger Trx2 overexpression (Fig. 5g). This result agrees with other papers published by different groups, where Grx2 KO mouse model showed no overexpression of Trx2 [34,38,39], suggesting that no major redox compensatory mechanisms are activated and that Grx2a probably has a peculiar function in the mitochondrial physiology.

It was previously reported that mitochondrial fatty acid metabolism can be regulated via reversible protein S-nitrosylation, another PTM involving redox active cysteines [45]. In general, oxidative stress conditions were shown to increase obesity and liver fat deposition [46,47]. In addition, it was shown that, in obese subjects, levels of the mitochondrial redox enzymes Gpx3 and Prx3 were decreased in adipose tissue [48,49]. Both Gpx3 and Prx3 are involved in the removal of hydrogen peroxide and therefore lack of their activity determines a shift toward a more oxidized status that seems to be responsible for the increased deposit of fat. Lipid accumulation in the liver is a major hallmark of MAFLD that is considered to have shared characteristics with obesity and the metabolic syndrome. Based on the data indicating a MAFLD phenotype, we investigated the expression levels of target genes that were previously described to be altered in MAFLD patients and we were able to detect different expression of several of these genes (Fig. 3). According to Ref. [50], the expression levels of *LDLR* and *SREBF2* were shown to be strongly reduced by 90 and 50%, respectively, in MAFLD patients. These findings are similar to what we measured in fasted mGD mouse livers. *SREBF2* expression in MAFLD is still controversial as it has been reported to be downregulated in MAFLD patients [30], while other authors reported no changes in the mRNA expression, but a stabilization at protein level [31,51].

Of note, the proteomic analysis showed some interesting results regarding the expression of enzymes of lipid metabolism (Table 4 and S1). Some of these genes (Cyp2e1, Cyp4a10 and Cyp4a14), found to be particularly abundant in mGD liver mitochondria, result associated with MAFLD [52] and hepatic steatosis [53]. In addition, Acyl-CoA thioesterase 2 (ACOT2) was found to be particularly abundant in the mitochondrial lysates of mGD mice (Table S1). ACOT constitutes a family of

enzymes that hydrolyze fatty acyl-CoAs to form free fatty acids and CoA. Some evidences suggest a regulatory role in controlling the rates of peroxisomal and mitochondrial acyl-CoA oxidation, as well as the subcellular trafficking of fatty acids. ACOTs are involved in the pathogenesis of metabolic diseases such as obesity, diabetes, and nonalcoholic fatty liver disease [54]. Furthermore, ACOT2 in the mitochondrial matrix can mitigate β-oxidation overload and maintain CoA availability [55]. Interestingly, ACOT2 overexpression causes a proton leak that could contributed to some degree to the uncoupling of respiration [56].

We also observed that Grx2a depletion highly affected mitochondrial activity, as a decrease in respiration was associated with organelle depolarization, increased permeability transition and a higher sensitivity to calcium-induced swelling. The decreased abundance of some constituents of the ETC complexes I, III and IV can partially explain the decrease in respiratory capacity of mGD mitochondria (see Table 4) and might be related to an imbalance in the iron handling in the mitochondrial compartment leading to a lower insertion of iron as a prosthetic group (Fig. 5a). In addition, reactive cysteines on specific subunits of complex I of the respiratory chain can undergo regulation by glutathionylation [1]. Accordingly, we found alterations in the glutathionylation state of different subunits of complex I (Fig. 7b) further supporting the fundamental role of this PTM in controlling the mitochondrial functionality. In particular, Cys531 and Cys704 of Ndufs1, which are close to the NADH binding site, were identified to undergo glutathionylation, possibly determining a conformational change of the complex and a diminished NADH oxidation [57]. Of note, the complex I subunits that we found to be putatively differentially glutathionylated in WT and mGD, have also been correlated to MAFLD [58].

As reported in Fig. 4, Grx2 depletion is also associated with morphological alterations of mitochondria. The *c* and donut shaped-mitochondria are probably an index of invaginations of their membranes giving rise to erythrocyte shaped organelles, as previously observed for uncoupled mitochondria [59]. Interestingly, in a recent paper it was reported that $Grx2^{-/-}$ muscle displays elongated mitochondria and structural alterations, indicating different functions of Grx2 in the mitochondrial matrix and in the fusion-fission cytosolic machinery [60]. In accordance with our data, TEM analysis of total $Grx2^{-/-}$ mouse ventricle cross sections showed mitochondria with an irregular morphology [33]. Also the mitochondrial calcium fluxes and related signaling appear nowadays more and more intimately associated with the redox signaling especially in mitochondria [61]. Our investigations are in line with these reports since the absence of a redox active protein leads to an increased sensitivity of mGD mitochondria to calcium induced swelling and depolarization.

Concerning glucose metabolism, in the present study we show that the depletion of mitochondrial Grx2 impairs glycogen synthesis in the liver, suggesting a mechanism in agreement with that reported by Wang et al. who showed that a burst of ROS stimulated the activity of the glycogen synthase kinase 3β (GSK3β) [62]. In turn, the increased activity of GSK3β can inhibit the synthesis of glycogen. AKT dephosphorylation at Ser473 can also be triggered by ROS [35,63]. Of note, Grx1 was found to mediate AKT activation in endothelial cells [64], thus the close relationship between glutaredoxins and AKT regulation is further confirmed in our mGD mouse model.

In conclusion, Grx2 is a critical factor in mitochondrial pathophysiology especially in the liver as its deficiency leads to alterations of hepatic glucose and lipid metabolism. Overall, the lack of Grx2 in mitochondria leads to a metabolic phenotype characterized by the accumulation of fat in the liver and the development of MAFLD.

Author contributions

L.C and M.P.R. conceived the research project. V.S. and L.C. designed and performed most of the experiments, analyzed the data and wrote the manuscript. A.F. and F.T. assisted with mitochondrial isolation and respiratory experiments. N.P. performed the glucose tolerance test. M.G. L. carried out the plasma measurements. I.B. performed the LC-MS/MS analysis. N.F., A.B., G.A. and A.H. contributed to the interpretation of the results and to the writing of the manuscript. M.P.R. supervised the project, was involved in planning and coordination of the work and in the writing of the final manuscript. All authors discussed the results and contributed to the final manuscript.

Declaration of interests

The authors declare no competing interests.

Acknowledgements

M.P.R. and V.S. acknowledge BIRD187299/18 and FINA (code U-GOV RIGO_FINA18_01) projects granted by University of Padova (Italy). Authors thank Dr. Federico Caicci head of DiBio Imaging Facility of the Dept. of Biology, University of Padova. Prof. Rigobello's group thanks Dr. Valentina Masola and Dr. Walter Giuriati of the Dept. of Biomedical Sciences, University of Padova for the help with the histochemical analyses. In addition, M.P.R. acknowledges Dr. Valentina Giorgio of the Dept. of Biomedical and Neuromotor Sciences, University of Bologna, for the fruitful discussion. L.C. and A.H were supported by the Cancerfonden (961), the Swedish Research Council Medicine (13X-3529). L.C. and A.H. acknowledges Prof. Elias Arnér, Dr. Aristi Fernandes, Dr. Alfredo Gimeneze-Cassina, for the fruitful discussion; Dr. Renato Alves and Shayida Maimaiti for the help in the primary hepatocytes and GTT analysis; Dr. Fernando Ogata for the primers design; Drs. Markus Dagnell and Åse Mattson for the final editing of the text. I.B. and G.A. wish to thank the Cassa di Risparmio di Padova e Rovigo (Cariparo) Holding for funding the acquisition of the LTQ-Orbitrap XL mass spectrometer.

Appendix A. Supplementary data

Supplementary data to this article can be found online at https://doi.org/10.1016/j.redox.2022.102277.

List of Abbreviations

Grx2	Glutaredoxin 2
MAFLD	metabolic dysfunction-associated fatty liver disease
PTM	post-translational modification
WT	wild type
mGD	whole-body mitochondrial Grx2 depleted
ORO	Oil Red O
TEM	Transmission Electron Microscope
Ldlr	Low-Density Lipoproteins Receptor
Srebf	Sterol Regulatory Element Binding Transcription Factor
Hmgcr	3-hydroxy-3-methyl-glutaryl-coenzyme A reductase
Cyp7a1	Cytochrome P-450 7a1
MLM	mouse liver mitochondria
EGTA	ethylene glycol-bis(β-aminoethyl ether)-N,N,N′,N'-tetraacetic acid
CsA	Cyclosporin A
Succ	succinate
Glu/mal	glutamate/malate
ROS	reactive oxygen species
HK4	hexokinase 4
PAS	Periodic Acid–Schiff
IPGTT	intraperitoneal glucose tolerance test
GSK3β	glycogen synthase kinase 3β
AKT	Protein kinase B
GS	glycogen synthase
FC	fold change

References

[1] S.M. Beer, E.R. Taylor, S.E. Brown, C.C. Dahm, N.J. Costa, M.J. Runswick, M. P. Murphy, Glutaredoxin 2 catalyzes the reversible oxidation and glutathionylation of mitochondrial membrane thiol proteins: implications for mitochondrial redox regulation and antioxidant defense, J. Biol. Chem. 279 (2004) 47939–47951.

[2] A. Folda, A. Citta, V. Scalcon, T. Cali, F. Zonta, G. Scutari, A. Bindoli, M. P. Rigobello, Mitochondrial thioredoxin system as a modulator of cyclophilin D redox state, Sci. Rep. 6 (2016) 23071.

[3] T.R. Hurd, R. Requejo, A. Filipovska, S. Brown, T.A. Prime, A.J. Robinson, I. M. Fearnley, M.P. Murphy, Complex I within oxidatively stressed bovine heart mitochondria is glutathionylated on Cys-531 and Cys-704 of the 75-kDa subunit - potential role of Cys residues in decreasing oxidative damage, J. Biol. Chem. 283 (2008) 24801–24815.

[4] K. Dominko, D. Dikic, Glutathionylation: a regulatory role of glutathione in physiological processes, Arh. Hig. Rada. Toksikol. 69 (2018) 1–24.

[5] C.L. Grek, J. Zhang, Y. Manevich, D.M. Townsend, K.D. Tew, Causes and consequences of cysteine S-glutathionylation, J. Biol. Chem. 288 (2013) 26497–26504.

[6] T.R. Hurd, N.J. Costa, C.C. Dahm, S.M. Beer, S.E. Brown, A. Filipovska, M. P. Murphy, Glutathionylation of mitochondrial proteins, Antioxidants Redox Signal. 7 (2005) 999–1010.

[7] V.N. Gladyshev, A. Liu, S.V. Novoselov, K. Krysan, Q.A. Sun, V.M. Kryukov, G. V. Kryukov, M.F. Lou, Identification and characterization of a new mammalian glutaredoxin (thioltransferase), Grx2. J Biol Chem 276 (2001) 30374–30380.

[8] M. Lundberg, C. Johansson, J. Chandra, M. Enoksson, G. Jacobsson, J. Ljung, M. Johansson, A. Holmgren, Cloning and expression of a novel human glutaredoxin (Grx2) with mitochondrial and nuclear isoforms, J. Biol. Chem. 276 (2001) 26269–26275.

[9] C. Hudemann, M.E. Lonn, J.R. Godoy, F. Zahedi Avval, F. Capani, A. Holmgren, C. H. Lillig, Identification, expression pattern, and characterization of mouse glutaredoxin 2 isoforms, Antioxidants Redox Signal. 11 (2009) 1–14.

[10] M.E. Lonn, C. Hudemann, C. Berndt, V. Cherkasov, F. Capani, A. Holmgren, C. H. Lillig, Expression pattern of human glutaredoxin 2 isoforms: identification and characterization of two testis/cancer cell-specific isoforms, Antioxidants Redox Signal. 10 (2008) 547–557.

[11] C.H. Lillig, C. Berndt, A. Holmgren, Glutaredoxin systems, Bba-Gen Subjects 1780 (2008) 1304–1317.

[12] C. Johansson, C.H. Lillig, A. Holmgren, Human mitochondrial glutaredoxin reduces S-glutathionylated proteins with high affinity accepting electrons from either glutathione or thioredoxin reductase, J. Biol. Chem. 279 (2004) 7537–7543.

[13] C. Johansson, K.L. Kavanagh, O. Gileadi, U. Oppermann, Reversible sequestration of active site cysteines in a 2Fe-2S-bridged dimer provides a mechanism for glutaredoxin 2 regulation in human mitochondria, J. Biol. Chem. 282 (2007) 3077–3082.

[14] C.H. Lillig, C. Berndt, O. Vergnolle, M.E. Lonn, C. Hudemann, E. Bill, A. Holmgren, Characterization of human glutaredoxin 2 as iron-sulfur protein: a possible role as redox sensor, P Natl Acad Sci USA 102 (2005) 8168–8173.

[15] V. Scalcon, F. Tonolo, A. Folda, A. Bindoli, M.P. Rigobello, Dimers of glutaredoxin 2 as mitochondrial redox sensors in selenite-induced oxidative stress, Metallomics 11 (2019) 1241–1251.

[16] M. Eslam, P.N. Newsome, S.K. Sarin, Q.M. Anstee, G. Targher, M. Romero-Gomez, S. Zelber-Sagi, V.W.S. Wong, J.F. Dufour, J.M. Schattenberg, et al., A new definition for metabolic dysfunction-associated fatty liver disease: an international expert consensus statement, J. Hepatol. 73 (2020) 202–209.

[17] Z. Younossi, Q.M. Anstee, M. Marietti, T. Hardy, L. Henry, M. Eslam, J. George, E. Bugianesi, Global burden of NAFLD and NASH: trends, predictions, risk factors and prevention, Nat. Rev. Gastroenterol. Hepatol. 15 (2018) 11–20.

[18] Z.M. Younossi, A.B. Koenig, D. Abdelatif, Y. Fazel, L. Henry, M. Wymer, Global epidemiology of nonalcoholic fatty liver disease-Meta-analytic assessment of prevalence, incidence, and outcomes, Hepatology 64 (2016) 73–84.

[19] D.K. Myers, E.C. Slater, The enzymic hydrolysis of adenosine triphosphate by liver mitochondria. I. Activities at different pH values, Biochem. J. 67 (1957) 558–572.

[20] I. Amigo, J. Traba, C.B. Rueda, Isolating brain mitochondria by differential centrifugation, Bio protocols 6 (2016), e1809.

[21] M.M. Bradford, A rapid and sensitive method for the quantitation of microgram quantities of protein utilizing the principle of protein-dye binding, Anal. Biochem. 72 (1976) 248–254.

[22] A. Mehlem, C.E. Hagberg, L. Muhl, U. Eriksson, A. Falkevall, Imaging of neutral lipids by oil red O for analyzing the metabolic status in health and disease, Nat. Protoc. 8 (2013) 1149–1154.

[23] G.L. Ellman, Tissue sulfhydryl groups, Arch. Biochem. Biophys. 82 (1959) 70–77.

[24] F. Tietze, Enzymic method for quantitative determination of nanogram amounts of total and oxidized glutathione: applications to mammalian blood and other tissues, Anal. Biochem. 27 (1969) 502–522.

[25] J.J. Mieyal, D.W. Starke, S.A. Gravina, C. Dothey, J.S. Chung, Thioltransferase in human red blood cells: purification and properties, Biochemistry 30 (1991) 6088–6097.

[26] N. Raghavachari, M.F. Lou, Evidence for the presence of thioltransferase in the lens, Exp. Eye Res. 63 (1996) 433–441.

[27] T. TeSlaa, M.A. Teitell, Techniques to monitor glycolysis, Methods Enzymol. 542 (2014) 91–114.

[28] E. Shulman, V. Belakhov, G. Wei, A. Kendall, E.G. Meyron-Holtz, D. Ben-Shachar, J. Schacht, T. Baasov, Designer aminoglycosides that selectively inhibit cytoplasmic rather than mitochondrial ribosomes show decreased ototoxicity A strategy for the treatment OF genetic diseases, J. Biol. Chem. 289 (2014) 2318–2330.

[29] V. Branco, L. Coppo, S. Sola, J. Lu, C.M.P. Rodrigues, A. Holmgren, C. Carvalho, Impaired cross-talk between the thioredoxin and glutathione systems is related to ASK-1 mediated apoptosis in neuronal cells exposed to mercury, Redox Biol. 13 (2017) 278–287.

[30] K. Fon Tacer, D. Rozman, Nonalcoholic Fatty liver disease: focus on lipoprotein and lipid deregulation, J Lipids 2011 (2011) 783976.

[31] H.K. Min, A. Kapoor, M. Fuchs, F. Mirshahi, H. Zhou, J. Maher, J. Kellum, R. Warnick, M.J. Contos, A.J. Sanyal, Increased hepatic synthesis and dysregulation of cholesterol metabolism is associated with the severity of nonalcoholic fatty liver disease, Cell Metabol. 15 (2012) 665–674.

[32] V. Howe, L.J. Sharpe, A.V. Prabhu, A.J. Brown, New insights into cellular cholesterol acquisition: promoter analysis of human HMGCR and SQLE, two key control enzymes in cholesterol synthesis, Biochim. Biophys. Acta Mol. Cell Biol. Lipids 1862 (2017) 647–657.

[33] G.N. Kanaan, B. Ichim, L. Gharibeh, W. Maharsy, D.A. Patten, J.Y. Xuan, A. Reunov, P. Marshall, J. Veinot, K. Menzies, et al., Glutaredoxin-2 controls cardiac mitochondrial dynamics and energetics in mice, and protects against human cardiac pathologies, Redox Biol. 14 (2018) 509–521.

[34] R.J. Mailloux, J.Y. Xuan, S. McBride, W. Maharsy, S. Thorn, C.E. Holterman, C. R. Kennedy, P. Rippstein, R. deKemp, J. da Silva, et al., Glutaredoxin-2 is required to control oxidative phosphorylation in cardiac muscle by mediating deglutathionylation reactions, J. Biol. Chem. 289 (2014) 14812–14828.

[35] J. Cao, D.Q. Xu, D.D. Wang, R. Wu, L. Zhang, H. Zhu, Q.J. He, B. Yang, ROS-driven Akt dephosphorylation at Ser-473 is involved in 4-HPR-mediated apoptosis in NB4 cells, Free Radical Biol. Med. 47 (2009) 536–547.

[36] S. Pietrobono, G. Anichini, C. Sala, F. Manetti, L.L. Almada, S. Pepe, R.M. Carr, B. D. Paradise, J.N. Sarkaria, J.I. Davila, et al., ST3GAL1 is a target of the SOX2-GLI1 transcriptional complex and promotes melanoma metastasis through AXL, Nat. Commun. 11 (2020), 5865.

[37] D. Szklarczyk, A.L. Gable, D. Lyon, A. Junge, S. Wyder, J. Huerta-Cepas, M. Simonovic, N.T. Doncheva, J.H. Morris, P. Bork, et al., STRING v11: protein-protein association networks with increased coverage, supporting functional discovery in genome-wide experimental datasets, Nucleic Acids Res. 47 (2019) D607–D613.

[38] R.J. Mailloux, J.Y. Xuan, B. Beauchamp, L.D. Jui, M. Lou, M.E. Harper, Glutaredoxin-2 is required to control proton leak through uncoupling protein-3, J. Biol. Chem. 288 (2013) 8365–8379.

[39] H.L. Wu, Y.B. Yu, L. David, Y.S. Ho, M.F. Lou, Glutaredoxin 2 (Grx2) gene deletion induces early onset of age-dependent cataracts in mice, J. Biol. Chem. 289 (2014) 36125–36139.

[40] Z. Wohua, X. Weiming, Glutaredoxin 2 (GRX2) deficiency exacerbates high fat diet (HFD)-induced insulin resistance, inflammation and mitochondrial dysfunction in brain injury: a mechanism involving GSK-3beta, Biomed. Pharmacother. 118 (2019) 108940.

[41] D. Shao, J. Han, X. Hou, J. Fry, J.B. Behring, F. Seta, M.T. Long, H.K. Roy, R. A. Cohen, R. Matsui, et al., Glutaredoxin-1 deficiency causes fatty liver and dyslipidemia by inhibiting sirtuin-1, Antioxidants Redox Signal. 27 (2017) 313–327.

[42] V. Scalcon, A. Bindoli, M.P. Rigobello, Significance of the mitochondrial thioredoxin reductase in cancer cells: an update on role, targets and inhibitors, Free Radical Biol. Med. 127 (2018) 62–79.

[43] N.M. Diotte, Y. Xiong, J.P. Gao, B.H.L. Chua, Y.S. Ho, Attenuation of doxorubicin-induced cardiac injury by mitochondrial glutaredoxin 2, Bba-Mol Cell Res 1793 (2009) 427–438.

[44] F.Q. Schafer, G.R. Buettner, Redox environment of the cell as viewed through the redox state of the glutathione disulfide/glutathione couple, Free Radical Biol. Med. 30 (2001) 1191–1212.

[45] P.T. Doulias, M. Tenopoulou, J.L. Greene, K. Raju, H. Ischiropoulos, Nitric oxide regulates mitochondrial fatty acid metabolism through reversible protein S-nitrosylation, Sci. Signal. 6 (2013) rs 1.

[46] B. Dewidar, S. Kahl, K. Pafili, M. Roden, Metabolic liver disease in diabetes - from mechanisms to clinical trials, Metabolism 111 (2020), 154299.

[47] I. Savini, M.V. Catani, D. Evangelista, V. Gasperi, L. Avigliano, Obesity-associated oxidative stress: strategies finalized to improve redox state, Int. J. Mol. Sci. 14 (2013) 10497–10538.

[48] J.Y. Huh, Y. Kim, J. Jeong, J. Park, I. Kim, K.H. Huh, Y.S. Kim, H.A. Woo, S. G. Rhee, K.J. Lee, et al., Peroxiredoxin 3 is a key molecule regulating adipocyte oxidative stress, mitochondrial biogenesis, and adipokine expression, Antioxidants Redox Signal. 16 (2012) 229–243.

[49] Y.S. Lee, A.Y. Kim, J.W. Choi, M. Kim, S. Yasue, H.J. Son, H. Masuzaki, K.S. Park, J. B. Kim, Dysregulation of adipose glutathione peroxidase 3 in obesity contributes to local and systemic oxidative stress, Mol. Endocrinol. 22 (2008) 2176–2189.

[50] M. Nakamuta, T. Fujino, R. Yada, M. Yada, K. Yasutake, T. Yoshimoto, N. Harada, N. Higuchi, M. Kato, M. Kohjima, et al., Impact of cholesterol metabolism and the LXR alpha-SREBP-1c pathway on nonalcoholic fatty liver disease, Int. J. Mol. Med. 23 (2009) 603–608.

[51] A.K. Madiraju, Y. Qiu, R.J. Perry, Y. Rahimi, X.M. Zhang, D. Zhang, J.G. Camporez, G.W. Cline, G.M. Butrico, B.E. Kemp, et al., Metformin inhibits gluconeogenesis via a redox-dependent mechanism in vivo, Nat. Med. 24 (2018) 1384–1394.

[52] M.A. Abdelmegeed, S.K. Ha, Y. Choi, M. Akbar, B.J. Song, Role of CYP2E1 in mitochondrial dysfunction and hepatic injury by alcohol and non-alcoholic substances, Curr. Mol. Pharmacol. 10 (2017) 207–225.

[53] X.Y. Zhang, S. Li, Y.F. Zhou, W. Su, X.Z. Ruan, B. Wang, F. Zheng, M. Warner, J. A. Gustafsson, Y.F. Guan, Ablation of cytochrome P450 omega-hydroxylase 4A14

gene attenuates hepatic steatosis and fibrosis, P Natl Acad Sci USA 114 (2017) 3181–3185.
[54] V. Tillander, S.E.H. Alexson, D.E. Cohen, Deactivating fatty acids: acyl-CoA thioesterase-mediated control of lipid metabolism, Trends Endocrin Met 28 (2017) 473–484.
[55] C. Bekeova, L. Anderson-Pullinger, K. Boye, F. Boos, Y. Sharpadskaya, J. M. Herrmann, E.L. Seifert, Multiple mitochondrial thioesterases have distinct tissue and substrate specificity, and CoA regulation, suggesting unique functional roles, J. Biol. Chem. 294 (2019) 19034–19047.
[56] C. Moffat, L. Bhatia, T. Nguyen, P. Lynch, M. Wang, D.N. Wang, O.R. Ilkayeva, X. L. Han, M.D. Hirschey, S.M. Claypool, et al., Acyl-CoA thioesterase-2 facilitates mitochondrial fatty acid oxidation in the liver, J. Lipid Res. 55 (2014) 2458–2470.
[57] J. Zhang, Z.W. Ye, S. Singh, D.M. Townsend, K.D. Tew, An evolving understanding of the S-glutathionylation cycle in pathways of redox regulation, Free Radical Biol. Med. 120 (2018) 204–216.
[58] A.M. Gusdon, K.X. Song, S. Qu, Nonalcoholic fatty liver disease: pathogenesis and therapeutics from a mitochondria-centric perspective, Oxid. Med. Cell. Longev. 2014 (2014), 637027.
[59] Y. Miyazono, S. Hirashima, N. Ishihara, J. Kusukawa, K. Nakamura, K. Ohta, Uncoupled mitochondria quickly shorten along their long axis to form indented spheroids, instead of rings, in a fission-independent manner, Sci Rep-Uk 8 (2018), 350.
[60] A. Liaghati, C.A. Pileggi, G. Parmar, D.A. Patten, N. Hadzimustafic, A. Cuillerier, K. J. Menzies, Y. Burelle, M.E. Harper, Grx2 regulates skeletal muscle mitochondrial structure and autophagy, Front. Physiol. 12 (2021) 604210.
[61] S. Feno, G. Butera, D.V. Reane, R. Rizzuto, A. Raffaello, Crosstalk between calcium and ROS in pathophysiological conditions, Oxid. Med. Cell. Longev. 2019 (2019), 9324018.
[62] Z. Wang, Y. Ge, H. Bao, L. Dworkin, A. Peng, R.J. Gong, Redox-sensitive glycogen synthase kinase 3 beta-directed control of mitochondrial permeability transition: rheostatic regulation of acute kidney injury, Free Radical Biol. Med. 65 (2013) 849–858.
[63] X. Li, F. Zhu, J.X. Jiang, C.Y. Sun, X. Wang, M. Shen, R. Tian, C.J. Shi, M. Xu, F. Peng, et al., Synergistic antitumor activity of withaferin A combined with oxaliplatin triggers reactive oxygen species-mediated inactivation of the PI3K/AKT pathway in human pancreatic cancer cells, Cancer Lett. 357 (2015) 219–230.
[64] J. Wang, S. Pan, B.C. Berk, Glutaredoxin mediates Akt and eNOS activation by flow in a glutathione reductase-dependent manner, Arterioscl Throm Vas 27 (2007) 1283–1288.